

**FUMED SILICA FILLED POLYURETHANEUREA
NANOCOMPOSITES**

ÇAĞLA KOŐAK

**KOÇ UNIVERSITY
AUGUST 2011**

Fumed Silica Filled Polyurethaneurea Nanocomposites

by

Çağla Koşak

**A Thesis Submitted to the
Graduate School of Sciences and Engineering
in Partial Fulfillment of the Requirements for
the Degree of**

**Master of Science
in
Materials Science and Engineering**

Koc University

August 2011

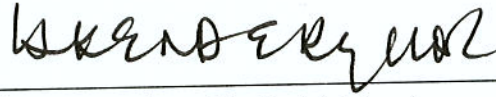
Koç University
Graduate School of Sciences and Engineering

This is to certify that I have examined this copy of a master's thesis by

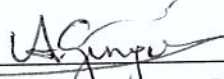
Çağla Koşak

and have found that it is complete and satisfactory in all respects,
and that any and all revisions required by the final
examining committee have been made.


Committee Members:



İskender Yılgör, Ph. D. (Advisor)



Atilla Güngör, Ph. D.



Yusuf Z. Menciloğlu, Ph. D.

Date:

Aug. 15, 2011

ABSTRACT

Novel, fumed silica filled thermoplastic polyether based and polydimethylsiloxane based segmented copolymers were synthesized and characterized. Polyether based polyurethaneureas were prepared by a two-step polymerization method from a cycloaliphatic diisocyanate, hydroxyl terminated poly(ethylene oxide) (PEO) and poly(tetramethylene oxide) (PTMO) with number average molecular weight of 2000 g/mol and 2-methyl-1,5-diaminopentane chain extender. Silicone-urea copolymers were synthesized from aminopropyl terminated polydimethylsiloxane (PDMS) oligomers with number average molecular weights of 32,000 and 2,500 g/mol and from cycloaliphatic diisocyanate in one step. Two different types of fumed silica HDK H2K (hydrophobic) and HDK N20 (hydrophilic) were incorporated into the segmented copolymers in amounts of 5-40% by weight. Influence of the silica type (hydrophilic versus hydrophobic), the amount of silica loading and the type of the soft segment on the morphology and tensile properties of the nanocomposites were determined. Major observations of this study were: (i) Incorporation of fumed silica affects the packing and organization in PEO and PTMO soft segments, (ii) incorporation of silica does not affect the glass transition temperature of PDMS, (iii) fumed silica incorporation interfere with the H-bonding of urea and urethane groups of segmented polyether based urethaneureas. (iv) Hydrogen bonding within the hard domains are disrupted upon fumed silica incorporation in polyether based polyurethaneureas. But, there is no difference in the H-bonding characteristics of the urea groups in the segmented silicone-urea copolymers. No change in the morphology of the corresponding nanocomposites are observed. (v) Incorporation of silica influences the tensile properties of silicone-urea segmented copolymers significantly, whereas the tensile properties of the polyether based systems do not improve upon fumed silica addition.

ÖZET

Polieter bazlı termoplastik kopolimerler ve termoplastik silikon-üre kopolimerleri sentezlendi ve karakterize edildi. Polieter bazlı poliüretanüreler halkalı alifatik diizosiyanat, molekül ağırlığı $\langle M_n \rangle$ 2,000 g/mol olan hidroksil sonlu poli(etilen oksit) (PEO) ya da poli(tetrametilen oksit) (PTMO) ve 2-metil-1,5-diaminopentan zincir uzatıcısı kullanılarak iki basamaklı “prepolimer yöntemi” ile sentezlendi. Silikon-üre kopolimerleri molekül ağırlığı $\langle M_n \rangle$ 2,500 ve 32,000 g/mol olan aminopropil sonlu polidimetilsiloksan (PDMS) ve halkalı alifatik diizosiyanat kullanılarak tek basamakta hazırlandı. HDK H2K (hidrofobik) ve HDK N20 (hidrofilik) olmak üzere iki çeşit amorf silika polimer ağırlığının % 5-40’ı kadar çok bloklu kopolimerlere eklendi. Amorf silika tipi (hidrofobik ya da hidrofilik), miktarı ve yumuşak kısım yapısının nanokompozit özellikleri ve çekme- kopma davranışlarına etkisi belirlendi. Çalışmadan elde ettiğimiz sonuçlar şunlardır: Amorf silika eklemek (i) PEO ve PTMO yumuşak kısımlarının kristalizasyonunu etkilemiştir, (ii) PDMS yumuşak kısmının camsı geçiş sıcaklığını değiştirmemiştir, (iii) polieter bazlı üretanüre kopolimerlerinin üretan ve üre kısımlarının birbirleriyle hidrojen bağlarını bir ölçüde engellemiştir. (iv) Sert kısımların hidrojen bağı yapıları amorf silika eklendikten sonra bozulmuştur. Fakat, silikon-üre kopolimerlerinin üre kısımlarının hidrojen bağlanma özelliklerinde amorf silika eklendikten sonra bir değişim gözlemlenmemiştir. Aynı polimerle hazırlanmış nanokompozitlerin de morfolojik özelliklerinde bir değişim gözlemlenmemiştir. (v) Amorf silika eklemek silikon-üre kopolimerlerinin çekme-kopma davranışlarını oldukça değiştirmiş fakat polieter bazlı sistemlerin çekme-kopma davranışlarında önemli bir etkiye sebep olmamıştır.

ACKNOWLEDGEMENTS

Many individuals have contributed to bring this project into happening and I would like to thank for their help over the last two years. Firstly, I would like to acknowledge my gratitude to my thesis advisors Prof. İskender Yılgör and Emel Yılgör for their endless support and patience throughout my research. Being a member of their research team under their precious guidance was a great opportunity for me.

I thank to all faculty members of Koc University Material Sciences and Engineering program for their help and teaching. I also thank to Prof. Yusuf Mencelođlu from Sabancı University for his guidance and very kind approach.

I like to thank to all members of Polymer research group. I also like to thank to the Ph.D. student Özge Malay from Sabancı Universty for her kind helps and supports.

I thank to Tübitak (The Scientific and Technological Research Council of Turkey) for the financial support.

I want to thank to my parents Gözde and Alkan Koşak, my grandfather Yalçın Oray for their never ending love, support and motivaton.

TABLE OF CONTENTS

List of Tables	vii
List of Figures	viii
Nomenclature	ix
Chapter 1: Introduction	1
1.1 Segmented Thermoplastic Polyurethaneureas.	2
1.2 Amorphous Fumed Silica.	8
1.3 Polymer Nanocomposites.	14
1.3.1 Preparation Methods for Nanocomposites.	16
1.3.2 Advantages of Polymeric Nanocomposites over Neat Polymers. . .	17
1.3.3 Examples of Important Fillers.	18
1.3.4 Possible Interactions between Fumed Silica and Neat Polymeric Matrix. .	19
Chapter 2: Experimental	25
2.1 Materials Used.	25
2.2 Polymer Syntheses.	29
2.2.1 Preparation of Poly(ethylene oxide) based Copolymers.	29
2.2.2 Preparation of Poly(tetramethylene oxide) based Copolymers. . . .	31
2.2.3 Preparation of Polydimethylsiloxane based Copolymers.	32
2.3 Preparation of the Samples for DLS Measurement.	32

2.4	Preparation of Polymer Nanocomposites.	33
2.5	Preparation of Model Compounds.	34
2.6	Instrumentation.	36
Chapter 3:	Results & Discussion	38
3.1	Model Studies: Investigation of the Behavior of Fumed Silica in Various Solvents and Model Compounds by Dynamic Light Scattering (DLS).	38
3.2	FTIR and ATR-IR Studies.	46
3.2.1	Model Studies.	49
3.2.1.1	FTIR Investigation of 1,3-Dimethylurea and Fumed Silica Mixtures.	49
3.2.1.2	ATR-IR Investigation of Poly(ethylene oxide) (PEO-2000) Fumed Silica Mixtures.	51
3.2.1.3	ATR-IR Investigation of Poly(tetramethylene oxide) PTMO-2000 and Fumed Silica Mixtures.	56
3.2.2.	FTIR and ATR-IR Investigation of PEO2-UU30 based Nanocomposites.	60
3.2.2.1	FTIR studies on PEO2-UU30 based Nanocomposites.	60
3.2.2.2	ATR-IR studies on PEO2-UU30 based Nanocomposites.	65
3.2.3.1	FTIR Spectra of PTMO2-UU20 based Nanocomposites.	68
3.2.3.2	ATR-IR Spectra of PTMO2-UU20 based Nanocomposites.	71
3.2.4	Silicone- urea based Nanocomposites.	73
3.3	The DSC Studies of the Oligomers.	74
3.4	Optical Microscopy Studies of Model Compounds.	75
3.5	X-Ray Diffraction (XRD) Studies.	76

3.6 Contact Angle Studies of Neat Polymers and Fumed Silica-Polymer Nanocomposites.81
3.7 Atomic Force Microscopy Studies.	83
3.8 Influence of Fumed Silica Filler on the Mechanical Properties of the Nanocomposites.86
Chapter 4. Conclusion	91
Bibliography	92
Vita	95

LIST OF TABLES

Table 2.1: Chemical structures of the reactants used in the synthesis reactions . . .	22
Table 2.2: Properties of hydrophilic (HDK N20) and hydrophobic (HDK H2K) fumed silica.	25
Table 3.1: Properties of different silica dispersions.	41
Table 3.2: DLS results of model compounds prepared with HDK H2K hydrophobic fumed silica	44
Table 3.3: DLS results of model compounds prepared with HDK N20 hydrophilic fumed silica.	44
Table 3.4: List of the polymers synthesized.	46
Table 3.5: Compositions of fumed silica polymer nanocomposites.	47
Table 3.6: DSC Results of the oligomers and mixtures.	75
Table 3.7: Static water contact angles on PTMO2-UU20 and PDMS32-U5 copolymers and their nanocomposites containing 10 and 40 weight % of fumed silica.	84
Table 3.8: Height and crosssection values of selected fumed silica agglomerates in the nanocomposites.	88
Table 3.9: Mechanical properties of the neat poly(ethylene oxide) based polyurethaneures and corresponding nanocomposites prepared.	89
Table 3.10: Mechanical properties of the neat poly(tetramethylene oxide) based polyurethaneures and corresponding nanocomposites prepared.	92
Table 3.11: Mechanical properties of the neat polydimethylsiloxane based polyurethaneures and corresponding nanocomposites prepared.	92

LIST OF FIGURES

Figure 1.1: Segmented Polyurethane consisting of alternating hard and soft segments.	3
Figure 1.2: Representation of hydrogen bonding between urethane and urea groups.	4
Figure 1.3: Representation of phase separation and phase mixing.	6
Figure 1.4: Production of hydrophilic fumed silica.	9
Figure 1.5: Production of hydrophobic fumed silica.	10
Figure 1.6: Representation of hydrophilic silica used in this work.	11
Figure 1.7: Representation of a hydrophobic silica obtained by surface modification.	12
Figure 2.1: FTIR spectra to monitor the progress of the PEO based polyurethaneurea synthesis.	26
Figure 3.1: DLS results for HDK H2K in: (A) THF and (B) IPA.	39
Figure 3.2: DLS results for HDK N20 in: (A) THF and (B) IPA.	40
Figure 3.3: DLS results for HDK H2K/DMU(1/1) in: (A) THF and (B) IPA.	42
Figure 3.4: DLS results for HDK N20/DMU(1/1) in: (A) THF and (B) IPA.	44
Figure 3.5: DLS results for (A) HDK H2K and (B) HDK N20 in D4/D5.	44
Figure 3.6: Carbonyl region in FTIR spectra of 1,3- DMU (red), 1,3-DMU/10% HDK N20 (purple), and 1,3-DMU/10%HDK N20 (blue).	50
Figure 3.7: ATR-IR Spectra of HDK N20 (blue) and HDK H2K (red) (A) 4000-700 cm^{-1} region, (B) 1500-700 cm^{-1} region.	50
Figure 3.8: FTIR spectra of PEO2000 and mixtures with various lodings of HDK	

H2K: red (neat), orange (1%), blue (5%), green (10%), and purple (20%).52
Figure 3.9: (A) 1300-1000 cm^{-1} and (B) 1000-700 cm^{-1} regions of model PEO-2000 mixtures with various loadings of HDK H2K: red (neat), orange (1%), blue (5%), green (10%) and purple (20%).53
Figure 3.10: (A) 1300-1000 cm^{-1} and (B)1000-700 cm^{-1} regions of the FTIR spectra for PEO-2000 mixtures with various loadings of HDK N20: red (neat), orange (1%), blue (5%), green (10%) and purple (20%).54
Figure 3.11: Schematic representations of gauche and trans forms in poly(ethylene oxide) chains.55
Figure 3.12: 1780-1680 cm^{-1} region of the FTIR spectra for PEO-2000 mixtures with HDK H2K (left) and HDK N20 (right) loadings: red (neat), orange (1%), blue (5%), green (10%), purple (20%).56
Figure 3.13: FTIR spectra of PTMO-2000 mixtures with various lodings of HDK H2K: red (neat), orange (1%), blue (5%), green (10%) and purple (20%).57
Figure 3.14: 1780-1680 cm^{-1} region of the FTIR spectra for PTMO-2000 mixtures with various HDK H2K loadings: red (neat), orange (1%), blue (5%), green (10%) purple (20%).57
Figure 3.15: (A) 1300-1000 cm^{-1} and (B) 1000-700 cm^{-1} regions of PTMO-2000 mixtures with various loadings: red (neat), orange (1% HDK H2K), blue (5% HDK H2K), green (10% HDK H2K), and purple (20% HDK H2K).58
Figure 3.16: (A) 1300-1000 cm^{-1} and (B) 1000-700 cm^{-1} regions of the FTIR spectra for PTMO-2000 blends with various loadings of HDK N20: red (neat), orange (1%), blue (5%), green (10%) and purple (20%).59
Figure 3.17: Various regions of the FTIR spectra of PEO2-UU30 and corresponding nanocomposites containing HDK H2K. (A) 3500-3100 cm^{-1} (B)3100-2600 cm^{-1} ,	

(C) 1800-1600 cm^{-1} , and (D) 1400-1000 cm^{-1} regions: red (neat), light blue (5%), blue (10%), green (20%), purple (40%).63
Figure 3.18: Various regions of the FTIR spectra of PEO2-UU30 and corresponding nanocomposites containing HDK N20. (A) 1800-1600 cm^{-1} , and (B) 1400-1000 cm^{-1} regions: red (neat), light blue (5%), blue (10%), green (20%), purple (40%).	64
Figure 3.19: ATR-IR spectra of PEO2-UU30 and its nanocomposites with HDK H2K (A)1800-1600 cm^{-1} , and (B) 1300-1000 cm^{-1} regions: red (neat), light blue (5%), blue (10%), green (20%), purple (40%).	66
Figure 3.20: ATR-IR spectra of PEO2-UU30 and its nanocomposites with HDK N20 (A)1800-1600 cm^{-1} , and (B) 1300-1000 cm^{-1} regions: red (neat), light blue (5%), blue (10%), green (20%), purple (40%).	67
Figure 3.21: FTIR spectra of PTMO2-UU20 and corresponding nanocomposites containing HDK H2K. (A) 3500-3100 cm^{-1} (B)3100-2600 cm^{-1} , (C) 1800-1600 cm^{-1} , and (D) 1400-1000 cm^{-1} regions: red (neat), light blue (5%), blue (10%), green (20%), purple (40%).	69
Figure 3.22: FTIR spectra of of PTMO2-UU20 and corresponding nanocomposites containing HDK N20. (A) 1800-1600 cm^{-1} and (B) 1400-1000 cm^{-1} regions: red (neat), orange (5%), blue (10%), green (20%), purple (40%).	70
Figure 3.23: ATR-IR spectra of neat polymer and corresponding nanocomposites in (A)3100-2600 cm^{-1} , (B) 1800-1600 cm^{-1} , and (C) 1400-1000 cm^{-1} regions: red (neat), light blue (5% HDK H2K), blue (10% HDK H2K), green (20% HDK H2K), purple (40% HDK H2K).	72
Figure 3.24: ATR-IR spectra of PTMO2-UU20 and corresponding nanocomposites in (A)3100-2600 cm^{-1} , (B) 1800-1600 cm^{-1} , and (C) 1400-1000 cm^{-1} regions: red (neat), light blue (5% HDK N20), blue (10% HDK N20), green (20% HDK N20), purple (40% HDK N20).	73

Figure 3.25: FTIR spectra of neat polymer and corresponding nanocomposites in (A) 1800-1500 cm^{-1} , (B) 1400-900 cm^{-1} regions: red (neat), light blue (5% HDK H2K), blue (10% HDK H2K), green (20% HDK H2K), purple (40% HDK H2K). .	75
Figure 3.26: Polarized OM images of A) 1,3-dimethylurea, B) 1,3-dimethylurea/10wt % HDK H2K, and C) 1,3-dimethylurea/HDK N20 with 10X magnification at RT.	77
Figure 3.27: XRD Spectra of hydrophilic HDK N20 (red) and hydrophobic HDK H2K (black).	79
Figure 3.28: XRD Spectra of PEO2-UU30 (red) and PEO2K (blue).	79
Figure 3.29: XRD Patterns of PEO2-UU30 (blue), and nanocomposites with HDK H2K 5% (red), 10% (green), 20% (purple) and 40% (light blue).	80
Figure 3.30: XRD Patterns of PEO2-UU30 (blue) and nanocomposites with HDK N20. 5% (red), 10% (green), 20% (purple) and 40% (light blue).	81
Figure 3.31: XRD patterns of PTMO2-UU20 (blue), and nanocomposites with HDK H2K. 5% (red), 10% (green), 20% (purple) and 40% (light blue).	82
Figure 3.32: XRD patterns of PTMO2-UU20 (blue), and nanocomposites with HDK N20. 5% (red), 10% (green), 20% (purple) and 40% (light blue).	82
Figure 3.33: Static water contact angles on air surfaces of (A) PTMO2-UU20 and its nanocomposites and (B) PDMS32-U5 and its nanocomposites	84
Figure 3.34. AFM Height Images of (A) PEO2-UU30/10wt% HDK H2K and (B) PEO2-UU30/ 10 wt% HDK N20.	86
Figure 3.35. AFM Height Images of (A) PTMO2-UU20/10wt% HDK H2K and (B) PTMO2-UU30/10 wt% HDK N20.	87

NOMENCLATURE

TPU	Thermoplastic polyurea and polyurethane
T _g	Glass transition temperature
HS	Hard segment
SS	Soft segment
CED	Cohesive energy density
δ	Solubility parameter
ΔU_{vap}	Energy of vaporization
PEO	Poly(ethylene oxide)
PTMO	Poly(tetramethylene oxide)
PDMS	Polydimethylsiloxane
R _g	Radius of gyration
HMDI	Bis(4-isocyanatocyclohexyl)methane
MDAP	2-Methyl-1,5-diaminopentane
DBDTL	Dibutyltin dilaurate
DMU	1,3-dimethylurea
IPA	Isopropyl alcohol
THF	Tetrahydrofuran
MEK	Methyl ethyl ketone
DMF	N,N-dimethylformamide
D4	Octamethylcyclotetrasiloxane
HDK N20	HDK N20 hydrophilic silica
HDK H2K	HDK H2000 hydrophobic silica
FTIR	Fourier Transform Infrared Spectroscopy

DLS	Dynamic light scattering
ATR-IR	Attenuated Total Reflectance Infrared Spectroscopy
T _m	Melting temperature
L ₀	Initial Length
DSC	Differential Scanning Calorimetry
XRD	X-Ray diffraction
OM	Optical microscopy
AFM	Atomic force microscopy
σ	Young's modulus
M	Modulus
TS	Tensile Strength
E	Elongation at break

Chapter 1

INTRODUCTION

Polymeric nanocomposites have been attracting widespread interest in the past 25 years due to dramatic improvement in various properties of the polymer-composite system. Studies by researchers at Toyota in 1980s have demonstrated dramatic increases in physical, thermal and mechanical properties of nylon-6/clay nanocomposites compared to unmodified nylon-6 [1,2,3]. These very positive results intensified the research in this field, where the main aim was to develop new organic-inorganic nanocomposites with optimized properties. A wide range of nanocomposites have been prepared by using different polymer matrices (thermoplastic or thermosetting) and inorganic fillers (alumina trihydrate, clays, talc, silica, montmorillonite, wollastonite and kaolin). By changing the composition, method of preparation (such as melt processing, solution mixing or in-situ polymerization), polymer matrix characteristics, nature, size, and shape of the filler material it is possible to manipulate the morphology and properties of nanocomposites. Nanocomposites have found applications in electronics, transportation, construction and communications industries, medicine and health and household goods.

In this research, our aim was to prepare fumed silica filled segmented thermoplastic polyurea and polyurethane (TPU) based nanocomposites and compare their morphology and properties with those of neat base polymers. Fumed silica is a frequently used filler in preparing nanocomposites because it provides increases in yield strength, elongation at break and modulus of the nanocomposite compared to various polymers, but especially to

silicones. In our studies we investigated the effect of soft segment structure and molecular weight in the TPU, amount of filler loading, and surface characteristics (hydrophilic or hydrophobic) of fumed silica on the properties of the composite materials. Subsequently, we tried to develop an understanding of the filler- matrix interactions in the systems and their effect on properties of the composites we have prepared.

1.1. Segmented Thermoplastic Polyurethaneureas

Thermoplastic elastomers constitute one of the most important and versatile classes of polymeric materials. Thermoplastic polyurethanes, polyurethaneureas and polyureas (TPU) are subcategory of thermoplastic elastomers. TPUs are segmented copolymers containing alternating hard and soft segments along a linear macromolecular backbone as shown in Figure 1.1.

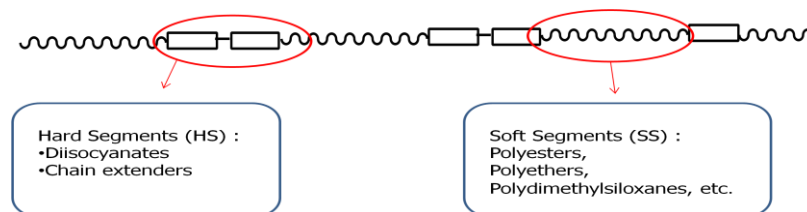


Figure 1.1. Segmented polyurethane consisting of alternating soft and hard segments

The soft segments in a TPU originate from hydroxyl or amine terminated oligomers with glass transition temperatures (T_g) well below room temperature; such as aliphatic polyethers, aliphatic polyesters, aliphatic polycarbonates, polydimethylsiloxanes, polyisobutylene, etc, whereas the hard segments consist of diisocyanate and a chain extender such as a low molecular weight diol or diamine. (e.g. butanediol or ethylene diamine) [4,5]. Availability of a very large selection of hard and soft segment constituents

and different synthetic techniques provide opportunities for the preparation of a wide range of TPU backbone structures. Each of the soft and hard segments gives different physical and chemical properties to the TPUs prepared from them [5].

The variables that have a strong effect on the structure and properties of segmented TPUs can be listed as follows:

- (i) chemical structure, number average molecular weight and molecular weight distribution of soft segments,
- (ii) chemical structure and symmetry of the diisocyanate and hard segments,
- (iii) chemical structure of the chain extender, average chain length and length distribution of hard segments,
- (iv) hard/soft segment ratio in the copolymer,
- (v) crystallizability of hard and soft segments,
- (vi) extent of competitive electrostatic interactions or hydrogen bonding between hard-hard and hard-soft segments,
- (vii) inherent miscibility of the hard and soft segments,
- (viii) polymerization procedure used during the synthesis (one-step versus two-step reaction), and
- (ix) thermal history of the polymer

Segmented TPUs generally display two-phase morphology, where soft segments constitute the flexible matrix and strongly hydrogen bonded hard segments act as reinforcing fillers. Hydrogen bonding between urethane and urea groups is schematically shown in Figure 1.2. As can be seen in the Figure 1.2., urea groups can form bifurcated hydrogen bonding, which is much stronger than the hydrogen bonding between urethane groups. Microphase separation in TPUs results in physical crosslinking between the hard segments, therefore,

unlike the conventional covalently crosslinked thermosets, segmented polyurethanes can be processed by thermal or solution methods [4].

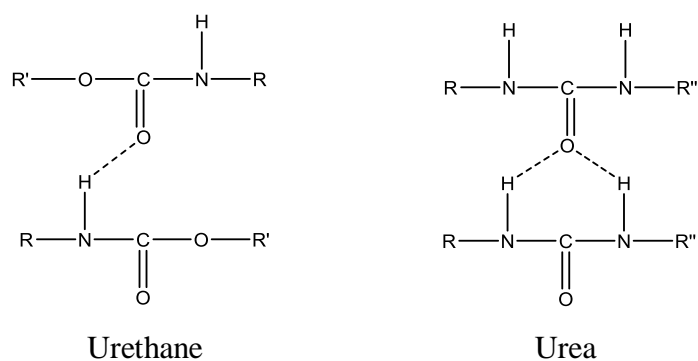


Figure 1.2. Representation of hydrogen bonding between urethane and urea groups

Microphase separation stems from the incompatibility of the soft and hard segments and/or crystallinity of the hard segment components [4]. The difference in the polarities of the hard and soft segments is one of the main factors which controls the incompatibility and thus leads to microphase separation. A good measure of the polarity of a group or molecule is the value of cohesive energy density (CED) or the solubility parameter (δ), which is the square root of CED [5].

$$\text{CED} = \frac{\Delta U_{\text{vap}}}{\text{Molar volume}}$$

$$\delta = \left[\frac{\Delta U_{\text{vap}}}{\text{Molar volume}} \right]^{1/2}$$

A large value of CED or δ indicates that the molecule is highly polar. The solubility parameter consists of three components, each component representing a different type of molecular interaction or intermolecular force. These components are δ_d due to dispersive (London) forces, δ_p due to dipole forces, and δ_h due to hydrogen bonding [4].

Solubility parameters of moderately polar poly(ethylene oxide) (PEO) and poly(tetramethylene oxide) (PTMO) are 9.0 and 8.6 (cal/cm³)^{1/2} respectively, whereas the solubility parameter of nonpolar polydimethylsiloxane (PDMS) is 7.6 (cal/cm³)^{1/2} [6]. Solubility parameters of highly polar and strongly hydrogen bonding urethane and urea groups are 14.2 and 16.8 (cal/cm³)^{1/2}, respectively [5].

Although the difference between the solubility parameters of polyether soft segments and polyurethaneurea hard segments give rise to phase separation between hard and soft segments in solid state, there is still a competition for H-bonding between the urethane or urea hard- and polyether (especially poly(ethylene oxide)) soft segments. This may lead to phase mixing and may strongly influence the mechanical properties and performance of these copolymers. On the other hand, silicone-urea copolymers with extremely non-polar PDMS soft segments and strongly polar urea groups as the hard segments exhibit excellent microphase separation, and fairly good elastomeric properties and mechanical strength. Figure 1.3 provides a schematic description of a well microphase separated and a phase-mixed polyurethane.

The hard segment is derived from association of urethane or urea units through strong H-bonding. Depending on the structure and symmetry of the diisocyanate and the chain extender, the hard segment can be glassy or semicrystalline. The ordered hard segments can act as bridges between the unordered soft segments [7] and reinforce the soft matrix by

acting as physical crosslinking sites. As the relative hard segment content of the copolymer is raised, the long range connectivity of the hard segments is thought to improve and lead to the percolation of the hard segments through the soft matrix. Intersegmental H-bonding capability of the hard segment and the potential crystallizability of the hard segment (if suitable symmetry exists) increase the cohesiveness of the hard domains. As a result the hard-segments are the major contributor of the modulus in TPUs [7] and it is documented that the strength and high elasticity of TPUs are because of the hard segments stabilized by H- bonding [5].

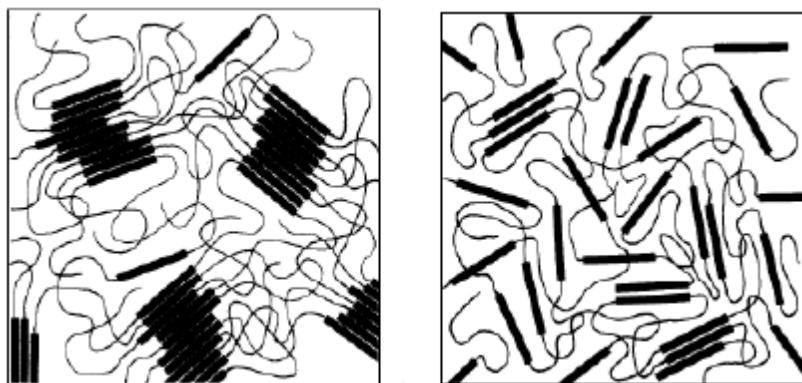


Figure 1.3. Representation of phase separation and phase mixing [9]

The soft segments consisting of flexible chains such as aliphatic polyether or polyester diols exhibit glass transition temperatures well below room temperature. The T_g of the soft segment is slightly higher than the T_g of their oligomers due to the restrictions imposed on the mobility of the soft segment by the hard domains as well as by isolated hard segments that may be dissolved in the soft matrix. The soft segments predominantly influence the elastic nature of a TPU [7,8].

Since their discovery in mid 50s [10, 11] multiphase, segmented TPUs are one of the most frequently investigated classes of polymers because of their wide range of properties. These polymers find applications in many different fields such as adhesives, protective coatings, biomaterials, textile fibers, high performance elastomers, etc. [5] Polyurethanes having poly(ethylene oxide) in their soft segment can be considered as hydrophilic because this oligomer is water soluble and water swellable. Hydrophilic polyurethanes find applications especially in biomaterials, protective wound dressings, and water resistant but water vapour permeable textile coatings [5].

PDMS based segmented TPUs display interesting combination of properties, which makes them good candidates for various interesting applications. The elastomeric properties of these copolymers are determined by the average PDMS molecular weight and PDMS content in the system [12], whereas their mechanical strength is mainly provided by the urea hard segments as mentioned previously [13]. Unique properties that are displayed by these copolymers include extremely low glass transition temperature of -123°C (therefore PDMS homopolymers exhibit very poor mechanical properties at room temperature even at high molecular weights), low surface energies, good thermal and oxidative stability, high gas permeability, low water absorption, physiological inertness, and blood and tissue compatibility. As a result of these properties, PDMS containing polymers find applications as speciality elastomers, biomaterials, anti-fouling marine coatings and high performance automotive coatings [12]. A major drawback of PDMS is that it exhibits very low mechanical properties as a result of their low T_g and very weak intermolecular forces between polymer chains. In order to reach reasonable mechanical properties PDMS must be crosslinked and filled with reinforcing fillers, if it is going to be

used in pure form [11]. Alternately, PDMS can be copolymerized with suitable organic hard segments, which can provide mechanical integrity to the copolymer [13, 14].

1.2. Amorphous Fumed Silica

Fumed silica is one of the most important fillers employed to reinforce polymeric materials. The discovery of fumed silica dates back to 1941 when Degussa patented a high temperature hydrolysis process of metallic oxides to produce extremely fine particle oxides. It was converted into a large scale production in 1950s and has become the process for preparation of nanoparticles based on silicon dioxide, aluminium oxide and titanium dioxide. Under TEM analyses, the primary particles of the three oxides show cubic forms with rounded off corners. All of these materials exhibit no internal surface. Fumed silica is marketed by various producers under the trade names of Aerosil, Cabosil and HDK [15]. Fumed (pyrogenic) silica is a white fluffy powder composed of aggregates of spherical primary particles, ca. 10 to 20 nm in diameter, which are fused together. These aggregates are assumed to be the primary structure of the filler in the suspensions. Agglomerates are clusters of aggregates linked by physical forces. [16]

Fumed silica is highly dispersed, amorphous, very pure silica that is produced by high temperature hydrolysis of silicon tetrachloride in an oxyhydrogen gas flame as shown in Figure 1.4. Pyrogenic silica and hydrogen chloride are formed by this hydrolysis at over 1000 °C. The SiO₂ primary particles about 5- 30 nanometers are produced at first. The primary particles are spherical and free of pores. In the flame, the primary particles fuse together permanently to form large units, or aggregates (100-1000 nm in size) which have a planar and angular structure. The aggregates are stable and cannot be disintegrated back to the primary particles, which means that the individual primary particles only exist in the

reaction zone itself. On cooling, the aggregates mechanically entangle reversibly to form agglomerates, known as tertiary structures. They are about 1-250 micrometers in size. In contrast to precipitated silica, fumed silica does not have a clearly defined agglomerate size. There is a large accessible surface area of the aggregates and agglomerates. This large surface area to mass ratio causes intense inter-particle interactions, which are result of attractive dispersion and dipolar forces. Fumed silica is insoluble in water and acids. However, it does dissolve in strong alkaline media to form silicates.

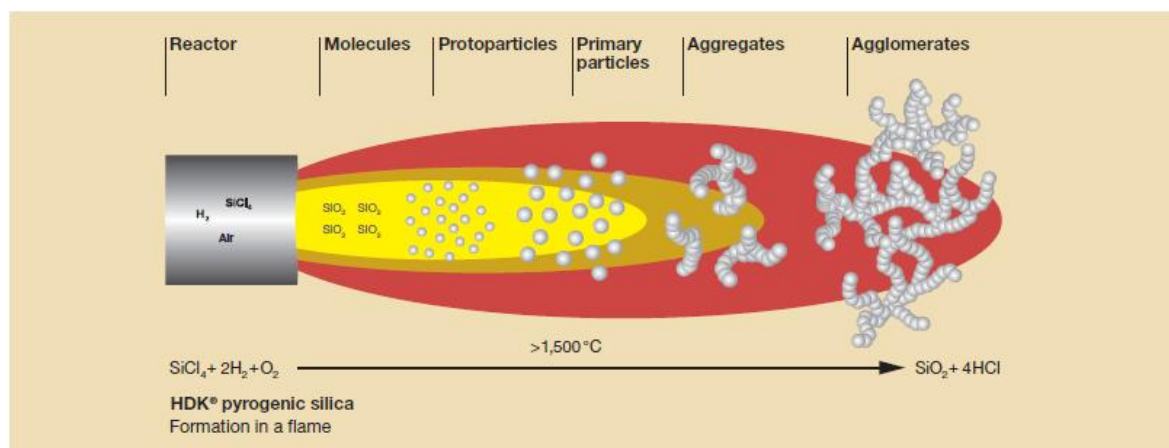


Figure 1.4. Production of hydrophilic fumed silica [17]

The untreated silica surface is partially hydrophobic and partially hydrophilic. Siloxane and silanol groups are situated on the surface. The latter is responsible for the hydrophilic behavior of the untreated fumed silica, whereas the nonpolar dimethylsiloxane and trimethylsiloxane groups account for the hydrophobic behavior. In literature, it is mentioned that there are three different types of surface silanol groups: (1) adjacent or H-bonded, (2) isolated, and (3) germinal [18]. The silanol groups, which can form hydrogen bonding, determine the interaction of fumed silica with solids, liquids, and gases.

The chemical nature of the silica surface can be readily changed by reaction with silanes. The reaction involves the chemical replacement of isolated silanol groups by organosilane groups through chemical grafting as shown in Figure 1.5. [18]. As a result, the following effects are expected:

- (1) Hydrophobicity of the nanoparticles is increased resulting in filler/matrix miscibility and more uniform dispersion.
- (2) The interfacial characteristics between the treated nanoparticles and the polymer matrix can be modified by selecting the desired coupling agents.

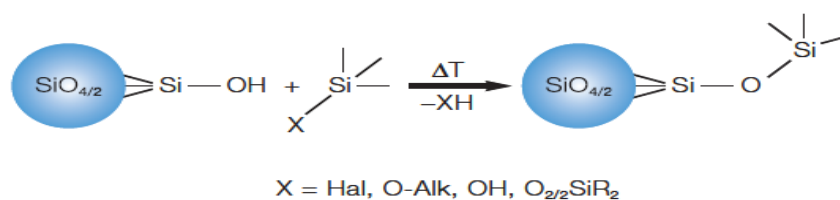


Figure 1.5. Production of hydrophobic fumed silica [19]

If the silica particles contain coupling agents, less aggregation takes place due to the presence of silane coupling agents, which promote a better dispersion of silica particles, improving the miscibility between the organic and inorganic phases since interparticle forces due to H-bonding are mainly responsible for reagglomeration [20, 21].

Schematic representation of the structures and various properties of hydrophobic and hydrophilic silica used in this work is provided in Figures 1.6. and 1.7.

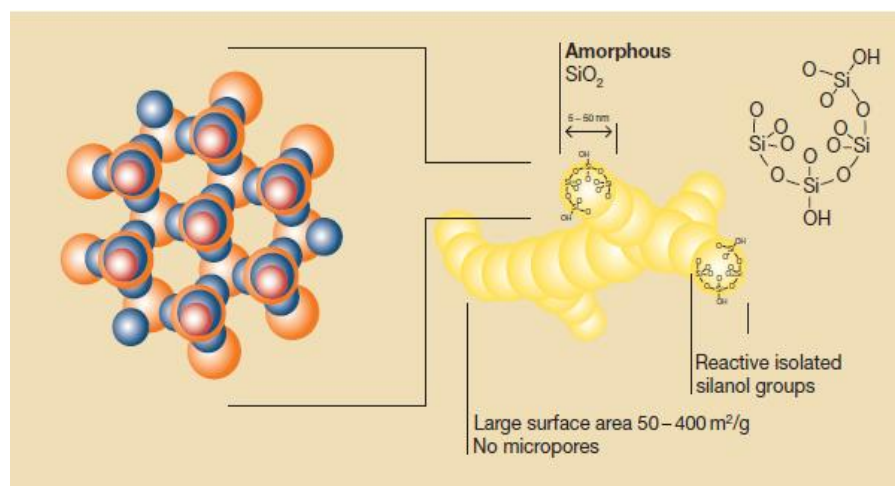


Figure 1.6. Representation of hydrophilic silica used in this work [19]

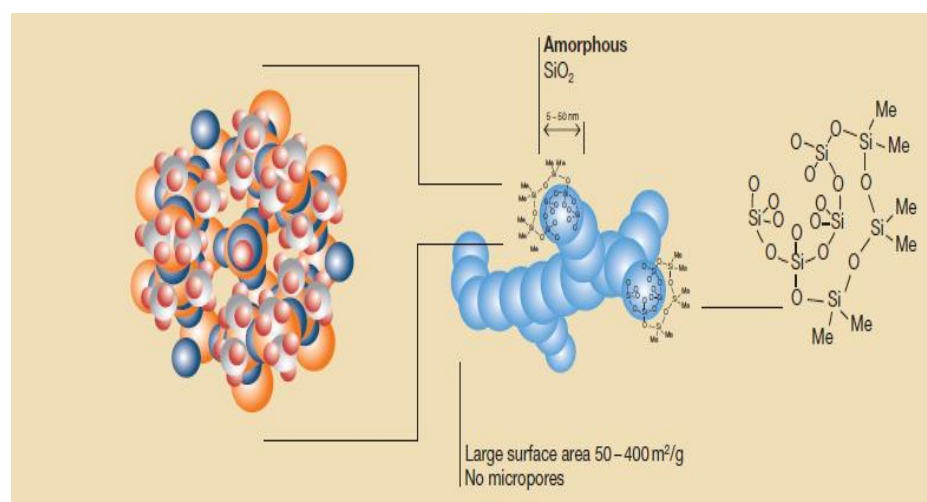


Figure 1.7. Representation of a hydrophobic silica obtained via surface modification [19]

Hydrophilic and hydrophobic grades of fumed silica are used in numerous applications such as a reinforcing filler, a thickening and thixotropic agent, an antisetling agent, and a free flow aid [22].

The reinforcing effect of particulate fillers on elastomers is generally considered to result in an: (1) Increase in the modulus, and (2) improvement in the fracture properties such as tensile strength, tear resistance, and abrasion resistance

The reinforcing effects of fumed silica on the polymer matrix mainly depend on:

1. Silica concentration,
2. Primary particle size,
3. Specific surface area, and
4. Interaction with the polymer matrix.

Silica concentration together with the filler loading determines the area available for interaction with the polymer matrix. Also large specific surface area and small primary particle size increase the area available for the interaction with the polymer matrix resulting an increase in the reinforcing effect [23]. The last factor also affects the influence of the first three properties and varies with the physical and chemical nature of both filler and the elastomer.

As a result of the factors mentioned above, the adhesion of the polymer to the filler surface is accomplished by forming a boundary layer of the matrix material on the surface of the filler. The thickness of the layer depends on the strength of the interaction, with a stronger interaction producing a greater thickness. The properties of a polymer in the boundary layer differ from those in the bulk of the matrix material primarily due to the decreased mobility

of the adsorbed chains on the filler surface. If the particles are closely spaced, the total mass of the matrix material may be located in the boundary layers, thus giving the matrix entirely different properties than are usual [24].

Since hard domains, which also act as crack propagating stoppers in soft elastomers, are globules, typically around 10-20 nm in diameter, the size of the fillers is comparable to that of hard domains. Therefore, an analogy between the function of the hard segment in the TPUs and the reinforcing effect of fillers has been drawn in literature, indicating that the block copolymers can be regarded as self-reinforcing [25]. The difference between silica and hard domain-filled TPUs is their morphology, the former does not change with increased filler concentration, while the domains of the latter become elongated to form rods or lamellae or become the continuous phase at high concentrations. Thus, nanosilica-filled systems may serve as model systems for testing the effect of concentration on properties without changing the morphology [23].

It is convenient to point out that improvements in mechanical properties of polyurethanes could also be achieved by synthesizing new polymers, whose hard segment concentrations are higher. That could be another way to increase the crosslinking density. Increase in urethane or urea concentration leads to an increase in the Young's modulus and hardness. However, this also increases the softening temperature of the material, and makes solution or melt processing more difficult. Other disadvantages may be a decrease in elongation at break, reduction in the flexibility at low temperatures, and difficulties encountered in polymer synthesis due to solubility problems as a result of increased hydrogen bonding. Therefore, addition of silica presents the advantages of the reinforcing effect of a filler without the disadvantages caused by the increase in hard segment concentration [25].

1.3. Polymer Nanocomposites

As discussed above already, in general two different approaches can be used to enhance the mechanical properties and thermal stability of TPUs:

1. Altering the molecular structure of the polyurethane (e. g. hard/soft segment ratio, structure of the hard segment, average molecular weight of the soft segment, etc.)
2. Introducing inorganic fillers to the polymer matrix. (Preparing composites)

In this study we mainly focused on using fumed silica fillers for property enhancement in TPUs.

Adding solid particles to polymers is a known method to produce tailored materials with enhanced properties with respect to the unfilled matrix. The resulting composite is a suspension of filler particles and/or agglomerates interspersed within the polymeric matrix. In a filled polymer containing micro-meter sized particles, high filler volume fractions are required to get significant changes of the macroscopic behavior. But, when the filler size is of the order of a few nanometers, considerable enhancements in properties can be potentially obtained even at low filler contents. Such improvements are the result of high interface between the phases resulting in more particle surface and particle-particle interactions [26,27].

Polymer nanocomposites consist of a nanoscale filler material (nanoparticle) and a polymeric matrix (e. g. thermoplastic, thermosets, or elastomers). A filled network may be regarded as a two phase system of rigid particles surrounded by an elastomeric network formed by flexible chains permanently linked together by physical junctions [28]. The

nanoparticle has at least one dimension in nanometer scale. It is added to the polymeric matrix in order to improve mechanical properties, gas barrier properties, thermal stability, fire retardancy, and other areas. There are many factors that affect the polymer nanocomposite properties. Some of these can be listed as follows:

1. Synthetic methods such as melt compounding, solvent blending, in-situ polymerization, and emulsion polymerization,
2. Polymer nanocomposite morphology,
3. Types of nanoparticles and their surface treatment,
4. Properties of the polymeric matrix such as crystallinity, molecular weight and polymer topology [22,29-31].

The use of inorganic particles as reinforcing materials for polymer melts is widespread in many commercial applications, in order to fabricate a large range of products, whose strength/weight and cost are at a premium [32].

1.3.1. Preparation Methods for Nanocomposites

After the selection of a particular polymer matrix and the appropriate nanoparticles for a specific application, the next challenge is to determine the proper synthesis method to create the desired polymer nanocomposite. The two most important challenges of polymer synthesis are:

1. Dispersing the particles from their agglomerated form into the matrix (in terms of activation energy), and

2. Maintaining the thermodynamic and kinetic stability of the final dispersion.

The choice of right preparation method is vital in overcoming these two problems. In general, for solid thermosetting reactive prepolymers or thermoplastic polymers with solid nanoparticles, the following processing methods are used:

1. Solution mixing (or intercalation)
2. Melt mixing (or intercalation)
3. Roll milling

On the other hand, for liquid thermosetting reactive prepolymers or thermoplastic polymers with solid nanoparticles, the following processing methods are used [22]:

1. In-situ polymerization,
2. Emulsion polymerization,
3. High-shear mixing

1.3.2. Advantages of Polymeric Nanocomposites over Neat Polymers

As mentioned before, nanoparticles provide improvements in various properties of the polymers such as:

1. Mechanical properties (tensile strength, stiffness, toughness)
2. Gas barrier,
3. Flame retardancy,
4. Dimensional stability,

5. Thermal expansion,
6. Ablation resistance,
7. Chemical resistance,

Improving the properties of polymers with fibrous or particle-reinforced polymer nanocomposites is achieved only if the dispersion of the nanoparticle and adhesion at the particle-matrix interface is sufficient. A good dispersion is achieved by increasing the adhesion between polymer and the filler. A poorly dispersed nanomaterial may reduce especially the mechanical properties. Additionally, by optimizing the interfacial bond between the particles and the matrix, the properties of the overall composite may be tailored [20].

However, there are also disadvantages of nanocomposites such as:

1. Increase in melt viscosity (limits processability),
2. Dispersion difficulties,
3. Optical Issues (clarity of films),
4. Sedimentation,
5. Black color when different carbon containing nanoparticles are used [20].

1.3.3. Examples of Important Fillers

There are many types of commercially available nanoparticles other than silica that can be incorporated into the polymer matrix to form polymer nanocomposites. Depending on the application, the researcher must determine the type of nanoparticle needed to provide the desired effect. Some of the most commonly used nanoparticles are:

1. Montmorillonite nanoclays (MMT),
2. Carbon nanofibers (CNFs),
3. Polyhedral oligomeric silsesquioxane (POSS),
4. Carbon nanotubes,
5. Nanosilica,
6. Nanoaluminium oxide (Al_2O_3),
7. Nanotitanium oxide (TiO_2) [20]

Fumed silica is chosen in this research as the reinforcing filler of the thermoplastic polyurethaneureas and polyureas synthesized.

1.3.4. Possible Interactions between Fumed Silica and the Polymeric Matrix

In recent years, composites of inorganic nanoparticles and polymers have received widespread interest. Most of the research focusing on the investigation of the filler/matrix interface, since it strongly influences the properties of the composite obtained. The nature of the interface has been used to divide these materials into two distinct classes:

1. Nanocomposites: Only weak bonds (hydrogen bonding, van der Waals, pi-pi bonds) between the matrix and the filler are present in nanocomposites.
2. Hybrids: The two phases are linked together through strong chemical bonds (covalent or ionic bonds). When covalent bonds are present between organic polymer matrix they are usually termed as hybrid materials [20].

The systems selected in our work are several polymers filled with very fine silica particles. These composite materials are expected to contain regions of restricted mobility due to the presence of polymer-filler interactions in terms of weak bonds.

Among different additives, fumed silica is a widely used filler made of primary particles of few nanometers. If the surface of particles is untreated, it is hydrophilic and the attractive interparticle forces play important role when dispersed within a polymeric matrix. If the viscosity of the suspending medium is low enough, the Brownian motion of the clusters becomes relevant and leads to formation of agglomerates, which eventually assemble to form a space-spanning network of clusters [26]. A completely hydrophilic surface may result incompatibility between the filler and the polymer matrix. A poor polymer-filler interaction would result in a dewetting (or cavitation) and vacuole formation upon a significant deformation thus initiating cracks. Therefore, a strong bond between particle and matrix significantly improves reinforcement. [26] On the other hand, the surface of the silica particles can be treated and made hydrophobic in order to increase the compatibility with the organic polymer chains and to decrease the agglomeration tendency of the nanoparticles. The consequence is that a percolating network is formed, based on the polymer bridging but also on direct particle-particle contact [33]. In both cases, the interactions at the interface between the polymer and the reinforcing additive change both the structure and mobility of the polymer within the interphase compared to the bulk. It is observed in literature that many polymer properties (viscosity, diffusion coefficient, NMR T2 relaxation time, glass transition temperature, etc.) in these interfacial regions are affected due to the restrictions on the mobility that the chains experience in the vicinity of the surfaces. Some possible causes of the chain mobility reduction include crowding or local ordering of chains at the interface as well as loss of configurational entropy of the polymer segments near the solid surface [32-34]. The mobility of the chain units adjacent

to the filler surface differs considerably from the bulk. Polymer adsorption also plays a major role in determining the rheological state of the filled systems. The types of interactions which are determined by polymer adsorption include:

1. Different kinds of entanglement interactions,
2. Polymer bridging between different particles [21].

Extent of reduced chain mobility depends on the particle surface area. Therefore, the reinforcing effect of a filler increases with decreasing particle size. Moreover, the results of various experiments in literature at different hydration levels predict that removal of water from the silica surface should cause a reduction in the segmental dynamics of the adsorbed polymer chains meaning that removing water from the fumed silica surface via heating causes stronger particle- polymer interactions.

During the formation of the elastomeric structure from the solutions of TPUs containing well dispersed silica particles, the particles may interact with the hard segments by H-bonding (between the silanol groups of the particle surface and the hard segments) which is called bridging of the hard segments. The particles may also interact with the carbonyl or oxygen units of the soft segment, especially in case of polyether and polyester based systems [35].

The primary reinforcing mechanism by which silica fillers are thought to alter the properties of siloxane-based polymeric materials is via H-bonding. [36] According to literature, strong multiple H-bonding between surface –OH groups of the fumed silica and the PDMS main chain occurs upon filler addition leading to a solid-like layer of 1-2 nm thickness irrespective of the PDMS end-group or whether the chains are grafted or just adsorbed.

Chains participating in the adsorbed layer and extending into the bulk melt, possibly bridging different particles or additionally participating in trapped entanglements, are responsible for the fact that a large part of the polymer matrix, much more than the comparably small fraction present in the adsorption layer, is dynamically constrained. The presence of such polymer bridges was assumed to be the reason for the viscosity increase of filled polymer fluids [37].

Thermodynamically stable dispersion of nanoparticles into a polymeric liquid is enhanced for systems where the radius of gyration of the linear polymer is greater than the radius of the nanoparticle. Direct particle-particle bridges, or at least topologically linked structure must be present for most of the polymer chains. This is possible because of the good filler dispersion, where apart from agglomerates, smaller isolated particles or small clusters must be dispersed through the matrix with distances on the order of the radius of gyration of the polymer (ca 10 nm). Dispersed nanoparticles swell the linear polymer chains, resulting in a polymer radius of gyration that grows with the nanoparticle volume fraction. It is proposed that this entropically unfavorable process is offset by an enthalpy gain due to an increase in molecular contacts at dispersed nanoparticle surfaces as compared with the surfaces of phase separated nanoparticles [36-38].

For a given silica and polymer pair and assuming perfect wetting, the amount of polymer adsorbed per unit weight of silica is independent of the concentration of filler. The situation should be different at high concentrations due to incomplete wetting of the silica surface and due to a larger number of shared chains. In both cases, the amount of adsorbed polymer per unit weight would be comparatively less [36].

The adsorption is considered as comprising those chains, which are present within the radius of gyration (R_g) of the surface. Several studies have indicated that this behaviour is indeed found [37]. The majority of high performance polymers involve a blend of macromolecules and solid filler particles, which serve to improve the properties of the polymeric matrix.

The difficulty in determining the phase behavior of copolymer/particle composites stems mainly from the presence of several length scales within the system:

1. Monomer size,
2. Particle size,
3. Radius of gyration of the polymer chain

In typical experiments, the nanoparticles are larger than the monomer units yet smaller than the radius of gyration of the chains [36].

In literature, the particle-matrix interaction of nanocomposites is mainly explained as formation of a network consisting of particles interacting with each other directly or by means of an elastomer attachment, in which the latter case the elastomer can be considered crosslinked by means of filler particles or aggregates. The silica aggregates interact with each other by H-bonding through the surface hydroxyl groups and van der Waals attraction while the silica polymer attraction is probably due to the H-bonding between the hydroxyl groups on the silica surface with oxygen atom on the polymer chains and with the carbonyl groups in hard segments. Through these interactions physical adsorption of polymer molecules on the solid surface occurs. Breaking of silica aggregates via sonication and mixing results in small amount of freshly created surfaces, which should be particularly active and contribute to the new interaction formation. This is to say that an elastic

nanocomposite compound can form which resembles a physically crosslinked system even in the absence of crosslinking agents like hard segments [18].

In our work we tried to understand how our findings correlate with the properties of nanocomposites found out through the literature survey. In our study of the silica filled TPU composites we mainly investigated the influence of methods used in composite preparation on the morphology and properties of the composites.

The material preparation involves the processing of the nanoparticles with the polymer matrix into a nanocomposite. In the next part, characterization experiments are followed, which are composed of structure analysis and property measurements. Structure analysis is carried out using microscopic and spectroscopic techniques in order to determine the degree and level of dispersion of the fumed silica particles in the polymer matrix. Property characterization depends on the individual application and in our case, mechanical properties are investigated. Throughout our studies we mainly focused on:

1. Investigation of the influence of the type and amount of silica filler on thermal and mechanical properties of poly(ethylene oxide), poly(tetramethylene oxide) based TPUs and silicone –urea copolymers
2. Developing an understanding of the nature of interactions between fumed silica filler and poly(ethylene oxide) and poly(tetramethylene oxide) based copolymers and silicone –urea copolymers

Chapter 2

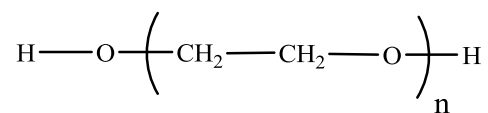
EXPERIMENTAL

2.1. Materials Used

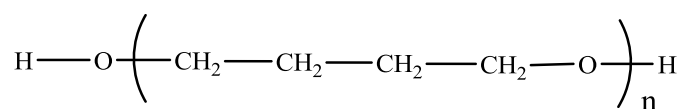
Poly(ethylene oxide) glycol (PEO) with $\langle M_n \rangle = 2,000$ g/mol was purchased from Merck. Poly(tetramethylene oxide) glycol (PTMO) with $\langle M_n \rangle = 2,000$ g/mol and chain extender 2-methyl-1,5- diaminopentane (MDAP) were kindly provided by DuPont. The diisocyanate, bis(4-isocyanatocyclohexyl)methane (HMDI) was kindly supplied by Bayer and had a purity better than 99.5%. Dibutyltin dilaurate (DBTDL) was obtained from Witco and is used as a catalyst by diluting to 1 weight % in tetrahydrofuran. Reagent grade 1,3-dimethylurea (DMU), isopropyl alcohol (IPA), tetrahydrofuran (THF), methyl ethyl ketone (MEK) and N,N-dimethylformamide (DMF) were obtained from Merck and were used as received. Octamethylcyclotetrasiloxane (D4) was obtained from Sivento- Degussa. α,ω -Aminopropyl terminated polydimethylsiloxane (PDMS) oligomers with $\langle M_n \rangle = 2,500$ and 31,500 g/mol were kindly provided by Wacker Chemie, München, Germany.

Chemical structures of the chemicals used are provided on Table 2.1.

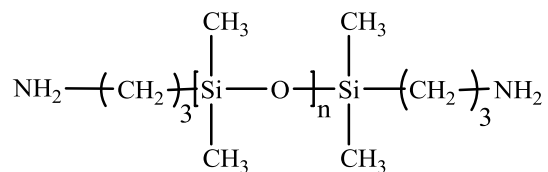
Hydrophilic (HDK N20) and hydrophobic (HDK H2000) fumed silica samples were kindly supplied by Wacker Chemie, München, Germany. Primary particle size of both silica types were 5-30 nm. Properties of the fumed silica used are given in Table 2.2.

Table 2.1. Chemical structures of the reactants used in the synthesis reactions

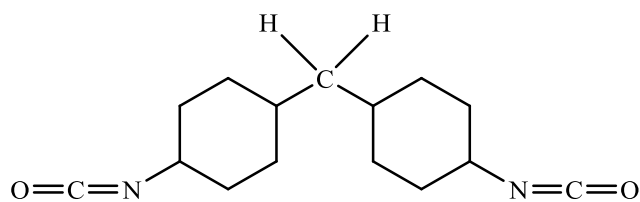
PEO: Poly(ethylene oxide), $M_n = 2,000$ g/mol



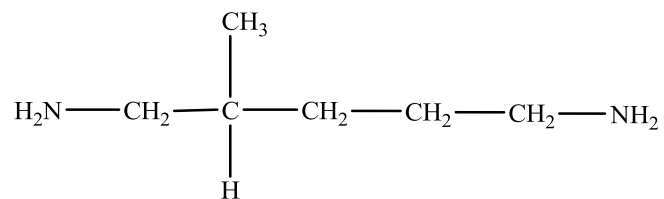
PTMO: Poly(tetramethylene oxide), $M_n = 2,000$ g/mol



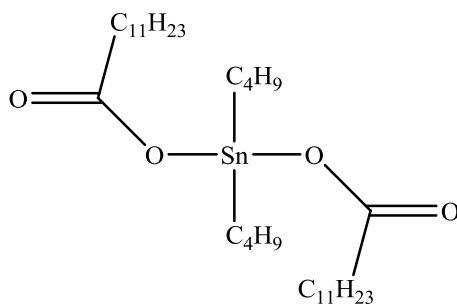
PDMS: α,ω -Aminopropyl terminated polydimethylsiloxane, $M_n = 2,500$ and $31,500$ g/mol



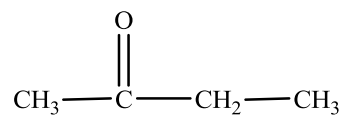
HMDI: Bis(4-cyclohexylmethane)diisocyanate



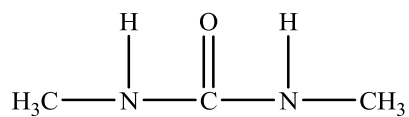
MDAP: (2-Methyl-1,5-diaminopentane)



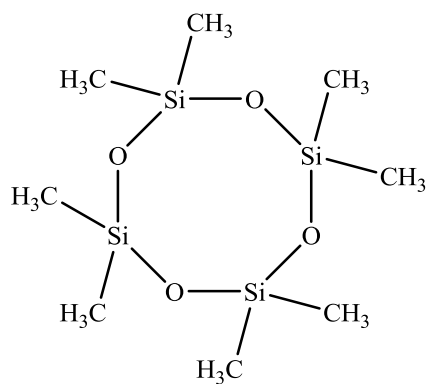
DBTDL: Dibutyltin dilaurate



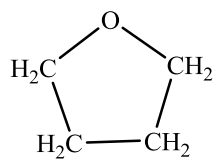
MEK: Methyl ethyl ketone



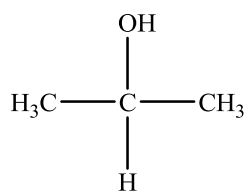
1,3 DMU: 1,3-Dimethylurea



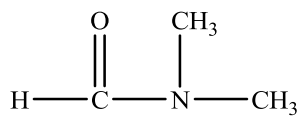
D4: octamethylcyclotetrasiloxane



THF: Tetrahydrofuran



IPA: Isopropyl alcohol



DMF: N,N-Dimethylformamide

Table 2.2. Properties of hydrophilic (N20) and hydrophobic (H2000) silica used

	HDK N20	HDK H2000
Silanol group density	2 SiOH/nm ²	0.25 SiOH/nm ²
BET surface	170-230 m ² /g	170-230 m ² /g
Surface modification	-	Trimethylsiloxy

2.2. Polymer Syntheses

2.2.1. Preparation of Poly(ethylene oxide) based Copolymers:

Polyurethaneurea segmented copolymers with 30 % by weight hard segment content were synthesized by using a two step polymerization method called the “prepolymer method”. All reactions were carried out in three-neck, round bottom, Pyrex reaction flasks equipped with a mechanical overhead stirrer, a thermometer and an addition funnel. Heating was provided by a heating mantle. For the preparation of isocyanate terminated prepolymer, calculated amounts of PEO and HMDI were put into the reaction flask, THF was added as solvent and the mixture is stirred at 60°C. DBTDL solution (1 weight % in THF) was used as catalyst. Completion of the prepolymer reaction was determined by FTIR (Fourier Transform Infrared) spectroscopy. In order to control the viscosity increase, THF was added to the prepolymer solution. Prepolymer reactions were completed in about 1 hour. The heat was then turned off and the prepolymer solution was cooled to room temperature.

In the second part of the polymerization reaction, which is called the “chain extension” step, the isocyanate terminated prepolymers were reacted with the chain extender by the

dropwise addition of stoichiometric amount of MDAP solution in DMF, at room temperature in about 1.5 hours. The viscosity increase was controlled by adding DMF into the reaction flask. Completion of the reaction was determined by FTIR spectroscopy by monitoring the disappearance of the strong isocyanate peak at 2260 cm^{-1} . The polymer solution obtained was cast in a Teflon mold. The mold was kept at room temperature for 24 hours and then placed in a vacuum oven at 60°C for 24 hours for complete evaporation of the solvent.

Following figure is an example to show how to monitor the progress of the polyurethaneurea synthesis by the FTIR spectra taken at different stages of the reaction.

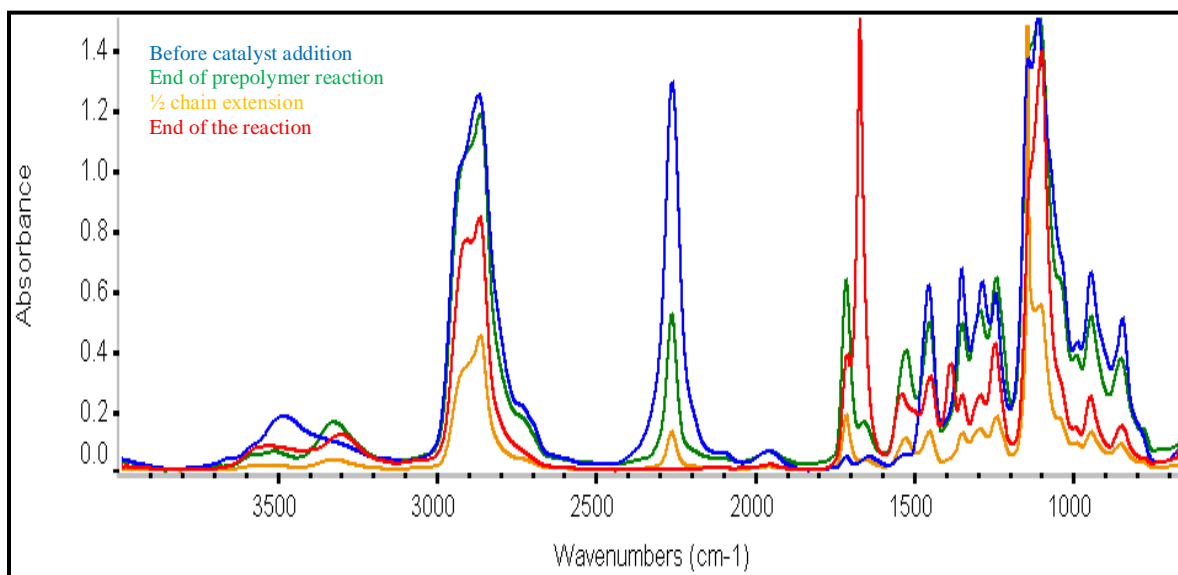


Figure 2.1. FTIR spectra were used to monitor the progress of the PEO based polyurethaneurea synthesis.

FTIR of the oligomer and diisocyanate mixture was first taken before catalyst addition and it was seen that there was a broad stretching peak at 3500 cm^{-1} representing the hydroxyl

group of the poly(ethylene oxide) oligomer. The peak at 2264 cm^{-1} because of the isocyanate stretching was very intense because only trace amount of isocyanate can react with hydroxyl groups in the reaction medium in the absence of catalyst. After adding the catalyst, spectra were taken at different time intervals and it was seen that at the end of the prepolymer reaction, a distinct peak at 3325 cm^{-1} appeared representing the N-H stretch of the urethane group formed. Since isocyanate and hydroxyl groups have been reacted the intensity of the peak at 2264 cm^{-1} was diminished. Moreover peak at 1717 cm^{-1} appeared due to the urethane carbonyl formation. The prepolymer reaction continued until no hydroxyl peak was detected in the spectrum.

Throughout the chain extension step, urethane carbonyl peak was growing continuously while the isocyanate peak became smaller in intensity. Additionally, urea carbonyl peak appeared at this step at 1667 cm^{-1} . The reaction is completed when all the isocyanate peak disappears. The spectrum of the completed polymer revealed shifts of N-H and carbonyl peaks to the lower wavenumbers indicating enhanced H-bonding. A broad N-H peak at 3304 cm^{-1} with urethane C=O peak at 1716 cm^{-1} and urea carbonyl peak at 1661 cm^{-1} with a shoulder at 1647 cm^{-1} were present in the final spectrum.

2.2.2. Preparation of Poly(tetramethylene oxide) based Copolymers:

The polyurethaneurea block copolymers with 20% by weight hard segment content were also synthesized by following the same two step polymerization procedure described above. The only difference was that the prepolymer reaction was conducted in bulk at 80°C , instead of THF solution at 60°C . Completion of the prepolymer reaction is determined by FTIR (Fourier Transform Infrared) spectroscopy. Prepolymer step was completed in about 60 minutes as before.

The prepolymer mixture was cooled to room temperature and diluted with IPA and THF. Chain extension was obtained at room temperature by dropwise addition MDAP solution in IPA in about 1.5 hours. The viscosity increase was controlled by addition of THF/IPA solution into the reaction flask, when necessary. Completion of the reaction was determined by FTIR spectroscopy. Polymer solution was cast in a Teflon mold and solvent was removed following the procedure described above.

2.2.3. Preparation of Polydimethylsiloxane-urea Copolymers

Polydimethylsiloxane-urea copolymers were synthesized in one step, using the same apparatus. Calculated amounts of PDMS and HMDI solutions were prepared. Amine terminated PDMS32 and PDMS2.5 were mixed at a 1/1 weight ratio and a homogenous solution was prepared in THF. HMDI solution was separately prepared with THF in the reactor. The PDMS solution was added dropwise from an addition funnel onto the HMDI solution into the reaction flask at room temperature. The completion of the prepolymer reaction was monitored by FTIR spectroscopy. The disappearance of the strong isocyanate peak at the FTIR spectrum indicated the completion of the reaction. Polymer solution was cast in a Teflon mold and solvent was removed following the procedure described above.

2.3. Preparation of the Samples for DLS Measurement

In order to investigate the behavior of the silica particles in dispersion (i. e. whether they coagulated or not), Dynamic Light Scattering (DLS) measurements were performed by preparing silica solutions with a concentration of 10 mg/10 mL. Both hydrophobic HDK H2000 and hydrophilic HDK N20 silica solutions were prepared in DMF, MEK, IPA, and THF by sonicating for 2 hours and further stirring with a magnetic bar for 24 hours. The

model compounds composed of silica/1,3-DMU and silica/D4 mixtures were also prepared using the same method.

2.4. Preparation of Polymer nanocomposites

The nanocomposites were prepared in three steps:

1. Preparation of polymer solution:

The polymer was dissolved in THF/IPA (1/1 by weight) solvent mixture to obtain a solution with 15 weight percent polymer. The solution was put into the oven at 55 °C for 2 hours and then was stirred for 15 minutes with a magnetic stirrer to get a completely homogenous solution.

2. Preparation of fumed silica dispersion:

Required amount of fumed silica is weighed into a jar and THF/IPA (1/1 by w) solvent mixture was added to obtain a dispersion containing 5 weight percent fumed silica. This dispersion is sonicated for 1 hour in a Bandelin Sonorex RK255H ultrasonic bath.

3. Preparation of nanocomposite films:

The fumed silica dispersion was added onto the polymer solution. The resulting mixture was stirred for 5 days and then sonicated for 2 hours in order to obtain a homogenous nanocomposite solution which contained about 10 weight percent polymer. The solution was cast in a Teflon mold and kept at room temperature for 24 hours. The molds were then placed into an air oven at 60°C until polymer films with constant weights were obtained. The films had a thickness of 0.3-0.5 mm.

2.5. Preparation of Fumed Silica Mixtures

In order to better understand the interactions between the silica and urethane and urea hard segments, model mixtures of DMU with 10 weight percent hydrophobic HDK H2000 and HDK N20 were prepared in THF. DMU was used as model since it mimics the urea group of the polyurethane. The mixtures were prepared as follows: DMU was dissolved in THF (8 weight % solid) and put into the oven at 60°C for 1 hour. Hydrophobic or hydrophilic silica dispersion was prepared in THF (1 weight % solid) and the dispersion was sonicated for 1 hour. Sonicated silica dispersion was poured onto the DMU solution. The resulting mixture was stirred for 2 hours and sonicated for 1 hour. FTIR spectra of the resulting mixtures were taken in order to observe the shifts especially in carbonyl region.

In order to understand the interaction between the silica and the polyether soft segments present in the TPU, PEO/silica mixtures were prepared in THF only and PTMO/silica mixtures were prepared both in THF and in IPA due to the poor solubility of PEO in IPA. The mixtures with 1 to 20 weight % silica were prepared as follows: PEO (or PTMO) was dissolved in THF (or in IPA) (8 weight % solid) and put into the oven at 60°C. Hydrophobic and hydrophilic silica dispersions were prepared in THF (or in IPA) and were sonicated for 1 hour. The sonicated silica dispersion was poured onto the PEO (or PTMO) solution. The resulting mixture was stirred for 2 additional hours and sonicated for 1 hour. Solvent in the samples was evaporated in the oven at 40°C for 24 hours. ATR-FTIR spectra of the resulting samples were taken in order to observe the peak shifts, which is a strong indication of the presence of an interaction.

2.6. Instrumentation

ARE magnetic stirrers were used to prepare homogenous polymer or fumed silica solutions.

Bandelin Sonorex RK 255H ultrasonic bath was used for sonication, which operates at 230 V, 180/840 W and at a frequency of 35 kHz.

IK Yellow Line DI25 Basic high shear mixer with 18 G rotor is used for stirring silica solutions. The instrument operates at 230 V, 600W and at 24000 rotation/min.

FTIR spectra were recorded on a Nicolet Impact 400D FT-IR Spectrometer. Solutions were cast on KBr discs and films were obtained after evaporating the solvent with an air gun. 32 scans were taken for each spectrum with a resolution of 2 cm^{-1} . Omnic 6.0 Software is used to monitor/analyze the spectra.

ATR-IR spectra were recorded on a thermo scientific Smart iTR Instrument with Diamond ATR crystal and with an incident angle of 42° . Omnic Software is used to monitor the spectra. 16 scans were taken for each spectrum with a resolution of 4 cm^{-1} .

Dynamic Light Scattering measurements were performed with Malvern ZetaSizer Nano-S Instrument with the software Nano-S. Glass cuvettes with square aperture were used as sample holders.

The glass transition temperatures and melting temperatures of the oligomers and blends were obtained using Netzsch DSC-204 instrument. All the measurements were performed under N_2 atmosphere. Samples at room temperature were first heated to 80°C at 10 K/min ,

stayed at 80°C for 10 minutes. Then, samples were cooled to -160°C at 10K/min and stayed at that temperature for 10 min. Lastly, samples were heated to 80°C again and corresponding T_g and T_m values were achieved.

Bruker D2 Phaser XRD with Lynx Eye Detector is used in the X-Ray Diffraction analyses. The spectra were taken with Bragg-Brentano Focus Geometry and DiffracEva was used as Software. The X-Ray generator is Cu K α radiation source with a wavelength of 0.15418 nm. The source works at 30 kV and 10 mA. The width of the slit used is 1 cm. Beam angle is variable and begins at $2\theta = -4^\circ$ with a variable rotation of the sample holder at 40 turns/min. A spectrum with a range of $2\theta = 5$ to 80° is obtained.

Nikon Eclipse Optical Microscope ME600 with LINKAM TNP, TMS94 Heating Stages is used for Optical Microscopy experiments. Both polarized and nonpolarized images were taken with Kameram Software. Brightfield and darkfield options were used to obtain the best image. Spot software was used to monitor the images taken. Samples dropcast onto glass slides were first heated at a rate of 5°C/min to 140°C and then cooled down to the room temperature (24°C) with the same rate. Pictures of the monitored images were taken at different time intervals.

Krüss Contact Angle Goniometer G10 was used for the contact angle measurements. Kameram Software was used to take and display the contact angle pictures. 1 cc syringe with luer lock needle was used to put 20 μ l drops on the polymer samples. Distilled water was used as probe liquid. Contact angle of the water drop on the neat polymer and nanocomposite surfaces were measured using the static sessile drop method at $24 \pm 2^\circ\text{C}$. The average contact angle from 3 different location on each polymer and nanocomposite was determined with an average experimental error of about ± 3 degrees.

Atomic force microscopy (AFM) studies were undertaken using the Nanomagetics Instrument. The scans were performed in tapping mode using gold coated silicon probe NT-MDT NSG10, and both height and phase images were recorded. The tip of the probe has a spring constant of 5.5-22.5 N/m and a resonant frequency of 140-300 Hz. Both pure polymer and nanocomposite samples were diluted to 5% in THF/IPA solvent mixture prior to AFM studies. Then these solutions were spin-coated onto glass slides in order to have thin sample films. Height and phase images were simultaneously recorded on sample surfaces.

Stress-strain tests were performed on an Instron Model 4411 Tester. Series IX software is used. Dog-bone shaped specimens (ASTM D 1708) were cut from solution cast polymer films with $L_0 = 24.0$ mm. The thicknesses of the specimen were in the range of 0.3 to 0.5 mm. Tests were conducted at room temperature with a 25.0 mm/min cross-head speed. Three samples are tested for the same polymer and an average of Young's modulus, ultimate tensile strength, and elongation at break values were obtained.

Chapter 3

Results and Discussion

In this study preparation, characterization and structure-property behavior of fumed silica/polyurethaneurea nanocomposites were investigated. As mentioned earlier, two main objectives of this study are:

- (1) Investigation of the influence of the type and amount of silica filler on thermal and mechanical properties of; poly(ethylene oxide) (PEO), poly(tetramethylene oxide) (PTMO) and polydimethylsiloxane (PDMS) based thermoplastic polyurethaneurea copolymers,
- (2) Developing an understanding of the nature of interactions between fumed silica fillers and PEO, PTMO and PDMS based thermoplastic polyurethaneurea copolymers

3.1. Model Studies: Investigation of the Behavior of Fumed Silica in Various Solvents and Model Compounds by Dynamic Light Scattering (DLS)

In order to understand the distribution of hydrophilic and hydrophobic fumed silica in different media, model studies were performed by using Dynamic Light Scattering (DLS). DLS studies are useful and very informative in determining the size of the nanoparticles and understanding their behavior in different solvents. Before preparing nanocomposites, the right solvent should be chosen in order to obtain optimum dispersion of the nanoparticles. Both the size and the agglomeration tendency of the fumed silica in the

solvent will affect its interaction with the polymer matrix and as a result will have a strong role in the final properties of the nanocomposites. In this study, DLS was used to understand the agglomeration behavior of fumed, amorphous silica (both hydrophilic (HDK N20) and hydrophobic (HDK H2000)) with primary particle size of 10- 20 nm, in various solvents listed below. Silica concentration was constant at 10 mg/mL in all studies.

Silica dispersions in N,N-dimethylformamide (DMF), methyl ethyl ketone (MEK), isopropyl alcohol (IPA), and tetrahydrofuran (THF) were prepared according to the procedure provided in the experimental part. The solvents selected are typically used in the preparation/synthesis and/or dissolution of polyurethanes and polyureas. 5 measurements composed of 15 runs were taken for each sample.

Typical DLS distribution curves obtained for HDK H2K and HDK N20 in THF and IPA are reproduced in figures 3.1. and 3.2., respectively.

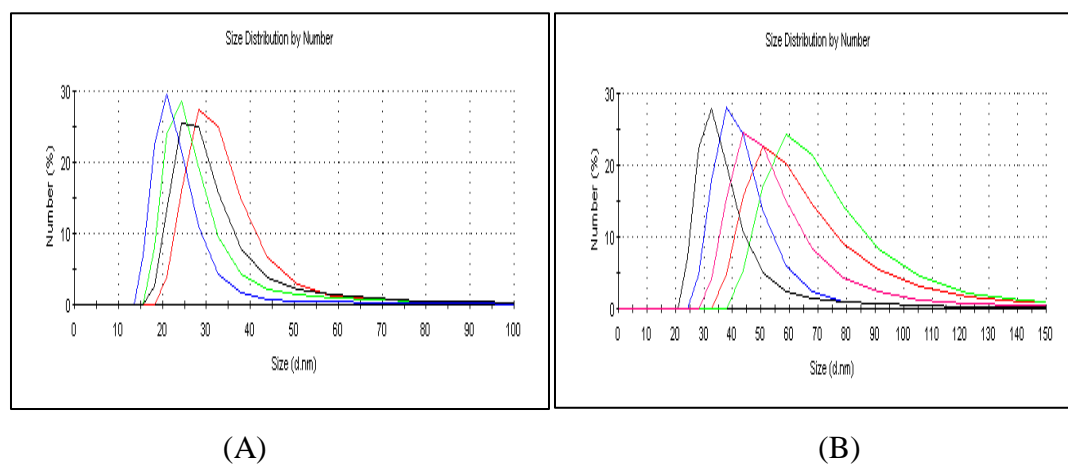


Figure 3.1. DLS results for HDK H2K in: (A) THF and (B) IPA

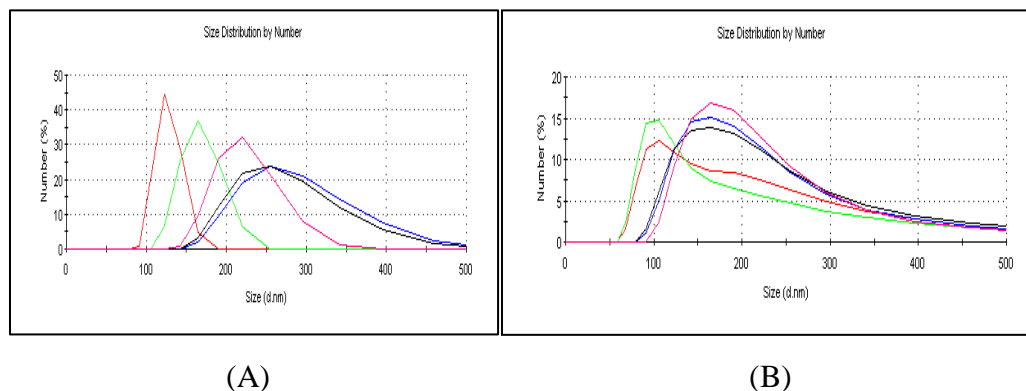


Figure 3.2. DLS results for HDK N20 in: (A) THF and (B) IPA

As can be seen in Figure 3.1. (A), hydrophobic silica (HDK H2K) gives a rather narrow and reproducible distribution in THF, with particle sizes in 20-30 nm. In IPA, a more polar solvent than THF, the particle size becomes broader and more dispersed (30 – 60 nm). Highly polar fumed silica (HDK N20) gives very large average particle sizes in THF (130 – 250 nm) and fairly broad size distribution, indicating strong agglomeration (Fig. 3.2. B). This may be expected, since THF is not a very polar solvent ($9.1 \text{ (cal/cm}^3)^{1/2}$). As shown in Fig. 3.2. B, the particle distribution is still fairly broad in IPA ($8.8 \text{ (cal/cm}^3)^{1/2}$), but average size is smaller (100 – 150 nm) when compared with that of THF.

Table 3.1. provides the number average size distribution results obtained from DLS studies for HDK N20 and HDK H2K in various solvents. Particle sizes of nearly 200 nm with large deviation values clearly shows that hydrophilic fumed silica (N20) tends to agglomerate more than the hydrophobic fumed silica in given solvents. This is because of the strong particle-particle interactions caused by the H-bonding of surface silanol groups. All the solvents except DMF seemed to be suitable for dispersing silica nanoparticles but, THF and IPA were chosen for nanocomposite preparation because they are also good solvents for

polyether and polydimethylsiloxane based copolymers. Another conclusion inferred from the DLS results was that the silica nanoparticles were present in the chosen solvents as clusters of 2- 20 primary particles. Low deviation values and good result qualities obtained were indications of a fairly good dispersion of the particle clusters of nearly same sizes for the hydrophobic fumed silica.

Table 3.1. DLS results of different silica dispersions.

Solution (10 mg/mL)	Average size (nm)
HDK N20 in DMF	too large agglomerate size resulting in experimental error
HDK H2K in DMF	28.8 ± 2.1
HDK N20 in MEK	150 ± 17
HDK H2K in MEK	23.6 ± 3.0
HDK N20 in IPA	210 ± 65
HDK H2K in IPA	54.4 ± 14
HDK N20 in THF	210 ± 24
HDK H2K in THF	44 ± 9.0

10 mg/mL dispersions of fumed silica in different solvents were also prepared by using IKA Yellow Line DI25 basic high shear mixer. Samples were stirred for both 5 and 15 minute intervals and their number averaged DLS results revealed that no change in average particle size was achieved by changing the method.

DLS studies were also performed with model compounds mimicking the hard and soft segments of the polymeric matrix, respectively. 1,3-dimethylurea (DMU) was used as a model for the hard segment, whereas octamethylcyclotetrasiloxane (D4) was used as

polydimethylsiloxane soft segment model and tetrahydrofuran (THF) was used as polyether soft segment model besides being a solvent. The aim was to understand the behavior of silica nanoparticles in hard and soft segments. DLS distribution curves obtained are reproduced in Figure 3.3., Figure 3.4. and Figure 3.5. As can be seen from Figure 3.3., both THF and IPA seem to be good solvents to distribute HDK H2K in DMU. In both cases average particle size is in 30-80 nm range.

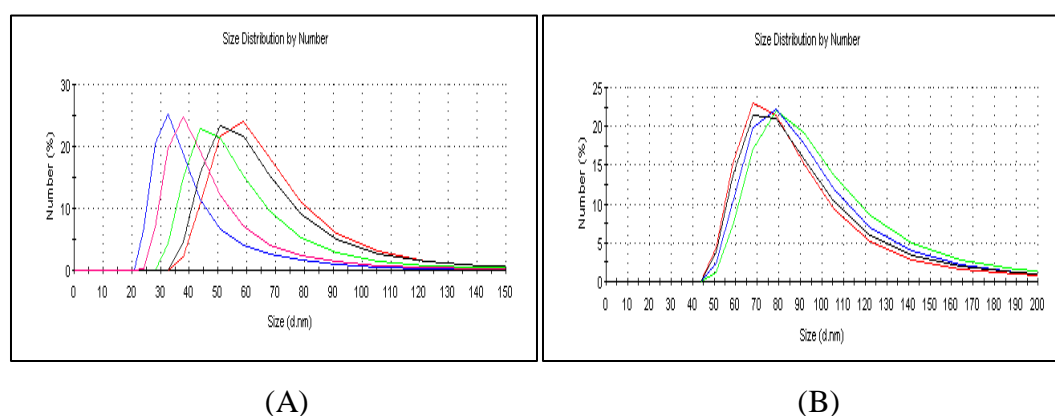


Figure 3.3. DLS results for HDK H2K/DMU(1/1) in: (A) THF and (B) IPA

On the other hand when hydrophilic silica is used HDK N20, the average particle size increased to about 100 nm in IPA and 150-200 nm range in THF, again showing some aggregation.

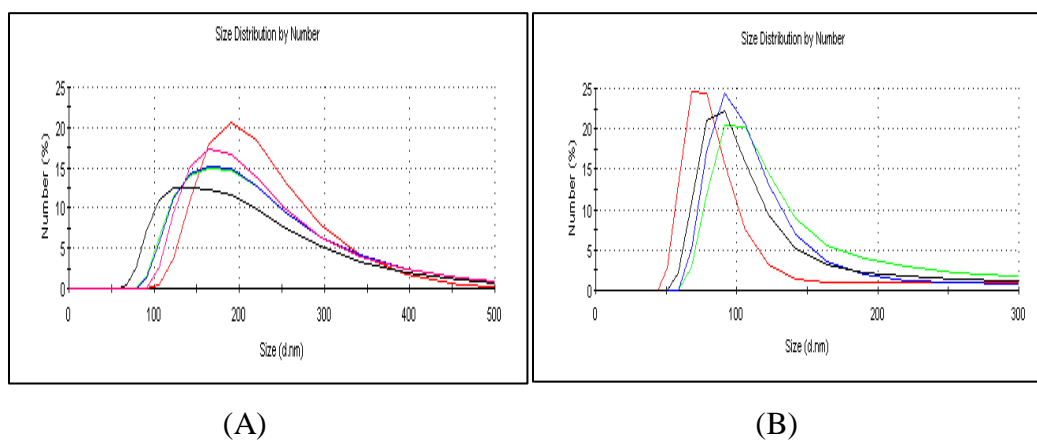


Figure 3.4. DLS results for HDK N20/DMU(1/1) in: (A) THF and (B) IPA

As shown in DLS curves provided in Figure 3.5. (A), distribution of hydrophobic silica (HDK H2K) in fairly nonpolar cyclic dimethylsiloxane (D4/D5) mixture is rather homogeneous with an average particle size in 25-80 nm range. This may be a good indication that HDK H2K will disperse well in PDMS and in silicone-urea copolymers. On the other hand, as can be seen in Figure 3.5. (B), hydrophilic silica N20 shows very strong aggregation in the same mixture with average particle size ranging from 250 to 1000 nm.

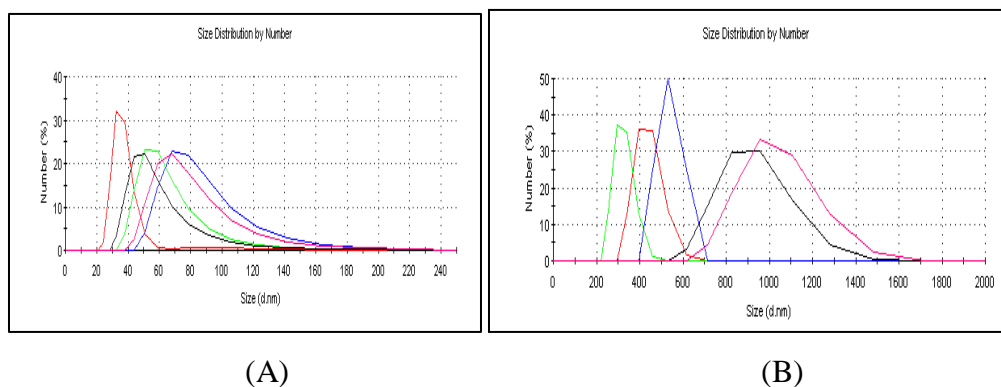


Figure 3.5. DLS results for (A) HDK H2K and (B) HDK N20 in D4/D5

These results may also indicate that distribution of N20 in silicone-urea copolymers may be somewhat problematic and may not be homogeneous. The number average size distribution results shown in Figures 3.3., 3.4. and 3.5., are summarized in Tables 3.2 and 3.3.

Table 3.2. DLS results of model compounds prepared with hydrophobic fumed silica

Material	Solvent/Model	Average size (nm)
HDK H2K	THF	44.2 ± 9.0
HDK H2K	IPA	54.4 ± 14
HDK H2K/1,3-DMU (1/1 by wt)	THF	53.3 ± 12
HDK H2K/1,3-DMU (1/1 by wt)	IPA	84.8 ± 10
HDK H2K/1,3-DMU (5/1 by wt)	THF	38.5 ± 2.0
HDK H2K/1,3-DMU (5/1 by wt)	IPA	85.5 ± 4.1
HDK H2K	D4/D5	64.0 ± 19

Table 3.3. DLS results of model compounds prepared with hydrophilic fumed silica

Solvent/Model	Solvent/Model	Average size (nm)
HDK N20	THF	370 ± 61
HDK N20	IPA	210 ± 61
HDK N20/1,3-DMU (1/1 by wt)	THF	201 ± 43
HDK N20/1,3-DMU (1/1 by wt)	IPA	203 ± 59
HDK N20/1,3-DMU (5/1 by wt)	THF	199 ± 12
HDK N20/1,3-DMU (5/1 by wt)	IPA	185 ± 85
HDK N20	D4/D5	550 ± 256

Next step in the study was to synthesize polymers which would be used in nanocomposite preparation. Polyurethaneureas based on poly(tetramethylene oxide) (PTMO), and poly(ethylene oxide) (PEO) as soft segments with $\langle M_n \rangle = 2000$ g/mol were prepared via two step polymerization method, whereas silicone-urea copolymers based on polydimethylsiloxane as soft segment were prepared by one stage method. Nanocomposites were prepared by adding 5, 10, 20, and 40 weight % of hydrophilic and hydrophobic fumed

silica into the polymers, respectively. However, in case of silicone-urea copolymers, only hydrophobic fumed silica was used as reinforcing filler and added in amounts of 10, 20, and 30 weight %. The trials made with hydrophilic silica failed due to the incompatibility of the polar silica surface with the nonpolar polydimethylsiloxane backbone, in line with the expectations from DLS results discussed previously.

List of the copolymers synthesized are provided in Table 3.4. The abbreviations used to identify the polymers is as follows: Capital letters indicate the type of soft segment in the copolymer, followed by its number average molecular weight and in kg/mole. U stands for urea and UU stands for urethaneurea. Last group of numbers indicate the hard segment content of the copolymer in weight percent. PEO2-UU-30, indicates a urethaneurea copolymer based on PEO-2000 with a hard segment content of 30% by weight. PDMS32-U-5 was prepared by using calculated amounts of PDMS-31500 and PDMS-2500 (1/1 by weight in soft segment) and HMDI, which constituted the hard segment.

Table 3.4. List of the polymers synthesized

Polymer Code	Soft Segment	Diisocyanate	Chain extender	HS Content (wt %)
PEO2-UU30	PEO-2000	HMDI	MDAP	30
PTMO2-UU20	PTMO-2000	HMDI	MDAP	20
PDMS32-U5	PDMS-31500 PDMS-2500	HMDI	-	5

PEO based polyurethaneureas contained 30 % hard segment by weight whereas PTMO based polyurethaneureas contained 20 % hard segment by weight. Our calculations revealed that there were 46 ether units per PEO chain in the first case whereas there were 28 ether units per PTMO segment chain in the latter case. Increase in the number of ether

units at constant soft segment molecular weight (46 in PEO, 28 in PTMO for oligomers with $\langle M_n \rangle = 2000$ g/mol) results in higher phase mixing due to increased ether-urethaneurea interaction. This is expected to weaken the mechanical properties of the polyurethaneurea prepared. In order to compensate this weakening effect, hard segment content of poly(ethylene oxide) based polyurethaneureas was increased. So, it was possible to compare the difference in mechanical properties of polyether based nanocomposites upon fumed silica incorporation with respect to neat polymers having similar mechanical properties. However, silicone-urea copolymer has different mechanical properties.

Hydrophilic (HDK N20) and hydrophobic (HDK H2K) fumed silica from Wacker Chemie were used as filler in nanocomposite preparation. Table 3.5. gives a list of the nanocomposites prepared and their compositions. Fumed silica content is given as weight and volume percent with respect to the polymeric matrix [(wt. silica/wt. polymer)x100] and the nanocomposite [(wt. silica/wt. polymer+wt.silica)x100], respectively. In the nomenclature, HDK N20 and HDK H2K indicate hydrophilic and hydrophobic fumed silica respectively. The numbers at the end give the amount of silica as weight percent. Bulk densities of polymers and fumed silica are taken as 1.0 and 2.2 g/cm³.

3.2. FTIR and ATR-IR Studies

In order to better understand the presence and extent of intermolecular interactions between fumed silica and polyurethaneurea matrix, we performed extensive investigations using Fourier Transform Infrared Spectroscopy (FTIR) and Attenuated Total Reflectance Infrared Spectroscopy (ATR-IR) on model systems and the composites prepared.

Table 3.5. Compositions of fumed silica/polymer nanocomposites

Sample	Silica				
	Type	in matrix		in nanocomposite	
		Amount (wt %)	Amount (vol %)	Amount (wt %)	Amount (vol %)
PEO2-UU30	-	-	-	-	-
PEO2-UU30/5%HDK H2K	HDK H2K	5	2.3	4.8	2.2
PEO2-UU30/10%HDK H2K	HDK H2K	10	4.5	9.1	4.3
PEO2-UU30/20%HDK H2K	HDK H2K	20	9.1	16.7	8.3
PEO2-UU30/40%HDK H2K	HDK H2K	40	18.2	28.6	15.4
PEO2-UU30/5%HDK N20	HDK N20	5	2.3	4.8	2.2
PEO2-UU30/10%HDK N20	HDK N20	10	4.5	9.1	4.3
PEO2-UU30/20%HDK N20	HDK N20	20	9.1	16.7	8.3
PEO2-UU30/40%HDK N20	HDK N20	40	18.2	28.6	15.4
PTMO2-UU20	-	-	-	-	-
PTMO2-UU20/5%HDK H2K	HDK H2K	5	2.3	4.8	2.2
PTMO2-UU20/10%HDK H2K	HDK H2K	10	4.5	9.1	4.3
PTMO2-UU20/20%HDK H2K	HDK H2K	20	9.1	16.7	8.3
PTMO2-UU20/40%HDK H2K	HDK H2K	40	18.2	28.6	15.4
PTMO2-UU20/5%HDK N20	HDK N20	5	2.3	4.8	2.2
PTMO2-UU20/10%HDK N20	HDK N20	10	4.5	9.1	4.3
PTMO2-UU20/20%HDK N20	HDK N20	20	9.1	16.7	8.3
PTMO2-UU20/40%HDK N20	HDK N20	40	18.2	28.6	15.4
PDMS32-U5	-	-	-	-	-
PDMS32-U5/10%HDK H2K	HDK H2K	10	4.5	9.1	4.3
PDMS32-U5/20%HDK H2K	HDK H2K	20	9.1	16.7	8.3
PDMS32-U5/30%HDK H2K	HDK H2K	30	13.6	23.1	12.0

In this study we were mainly focused on identifying the specific interactions between;

- (1) Urea and urethane hard segments and fumed silica,
- (2) Ether and siloxane linkages present in the soft segment backbones and fumed silica.

For this purpose we examined specific regions in the IR spectroscopy, where strong absorptions were observed by urethane and urea groups (specifically N-H and C=O absorption bands), and ether (C-O-C) and silicone (Si-O-Si) backbones. FTIR and ATR-IR are useful tools in determining the presence and the extent of possible interactions between fumed silica and polyether based polyurethaneureas or silicone-urea copolymers. Changes in the strong H-bonding character of polyurethaneurea matrix of the nanocomposites can be easily detected with the help of these techniques by comparing the spectra of unfilled and fumed silica filled samples. Peak shifts and shape changes especially at the carbonyl (C=O) ($1800 - 1500 \text{ cm}^{-1}$), ether (C-O-C) ($1200 - 1000 \text{ cm}^{-1}$) and silicone (Si-O-Si) ($1100 - 900 \text{ cm}^{-1}$) regions are indications of an interaction between the silica and the matrix in terms of H-bonding. For transmission FTIR studies KBr discs were used onto which the polymer or the nanocomposite solutions were dropcast. The solvent was evaporated with an air gun resulting in a thin film of specific sample on the KBr disc.

In case of ATR-IR studies the sample was put onto the single bounce diamond crystal of the ATR sampling accessory and the spectrum was taken. No solvent was required since the analysis of solids, pastes, or gels is possible with this method.

3.2.1. Model Studies

Model compounds both for the hard (1,3-dimethylurea, DMU) and the soft segments (PEO or PTMO oligomers) representing the segmented copolymers were used in model studies.

3.2.1.1. FTIR Investigation of 1,3-Dimethylurea and Fumed Silica Mixtures

1,3-Dimethylurea (DMU) is a very useful model compound to mimic the hard segments in silicone-urea copolymers. To investigate the presence of interactions between silica and the urea groups we prepared 10% by weight silica containing DMU blends designated respectively as DMU-H-10 and DMU-N-10 in THF, cast them on KBr discs and obtained their transmission FTIR spectra. The carbonyl region of the FTIR spectra for DMU and its blends with silica are reproduced in Figure 1. DMU shows a strongly hydrogen bonded C=O peak centered at 1624 cm^{-1} and two well defined shoulders at 1585 cm^{-1} (amide II, stretching) and 1537 cm^{-1} (amide II, vibration). As can be seen in Figure 3.6, FTIR spectra of DMU-H-10 and DMU-N-10 overlap completely and are also identical to that of DMU. Results of the FTIR studies do not indicate any significant change in the nature of the hydrogen bonded carbonyl groups in dimethylurea as a result of silica incorporation.

ATR-IR spectra of HDK N20 and HDK H2K shown in Figure 3.6. were taken before preparing the model mixtures of PEO and PTMO with fumed silica. An intense peak at 1085 cm^{-1} with a shoulder at 1205 cm^{-1} is detected for HDK N20, whereas an intense peak at 1075 cm^{-1} is detected for HDK H2K with a shoulder at 1205 cm^{-1} representing the Si-O-Si stretches.

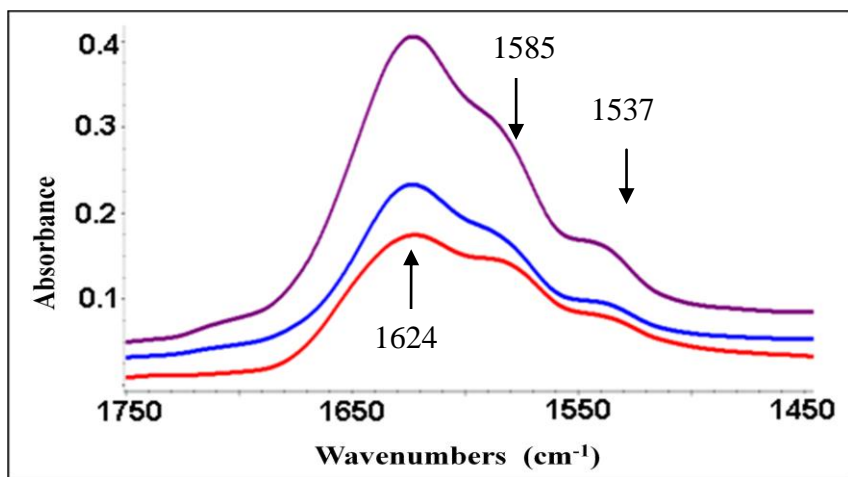


Figure 3.6. Carbonyl region in FTIR spectra of 1,3- DMU (red), 1,3-DMU/10% HDK N20 (purple), and 1,3-DMU/10%HDK N20 (blue)

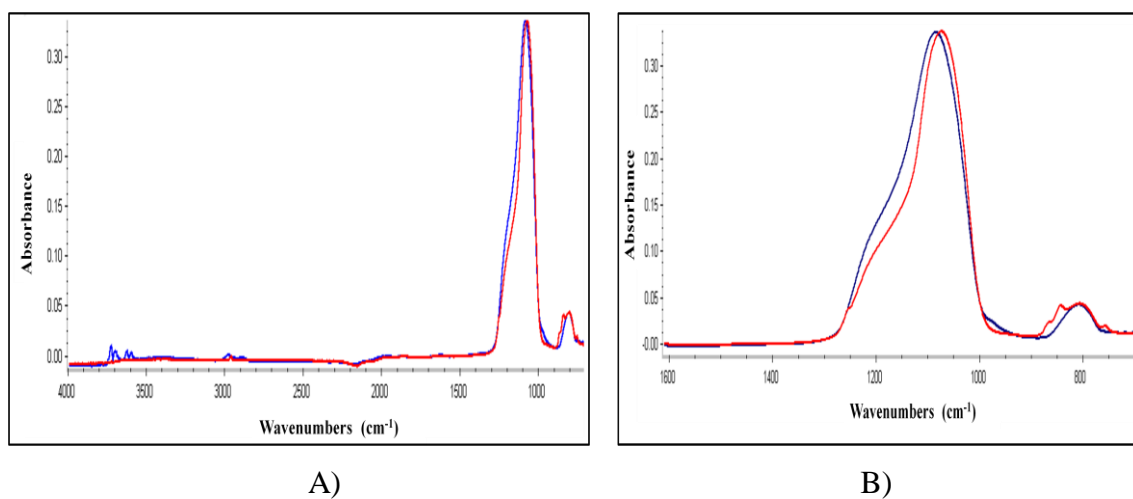


Figure 3.7. ATR-IR Spectra of HDK N20 (blue) and HDK H2K (red) (A) 4000-700 cm⁻¹ region, (B) 1500-700 cm⁻¹ region.

3.2.1.2. ATR-IR Investigation of Poly(ethylene oxide) (PEO-2000) Fumed Silica Mixtures

The mixtures were prepared at 1, 5, 10, and 20 weight % fumed silica (both hydrophilic and hydrophobic) loadings into oligomer solutions. We were mainly interested in finding out whether an interaction is present between C-O-C backbone of the soft segment and the hydroxyl groups on the hydrophilic silica surface. For this purpose, especially the region at 1200 to 1000 cm^{-1} range were closely examined. It was observed that difference in solvent used in the preparation step does not effect the spectrum obtained. Spectra of both air and mold sides of the samples were taken and it was seen that both sides revealed the same spectrum. Prior to the tests, we have assumed that fumed silica particles do not settle down due to gravity while drying the sample solutions in molds. This assumption was proven to be true by the similar spectra obtained from both sides of the samples.

FTIR spectra of PEO-2000 and its mixtures with various loadings of HDK H2K are reproduced in Figure 3.8. The hydroxyl peak of the oligomer centered at 3422 cm^{-1} was not affected by either hydrophobic (or hydrophilic) fumed silica incorporation. This was reasonable due to the very low amount of hydroxyl groups which are present only at the two ends of reasonably high molecular weight oligomer compared to the much higher numbers of C-O-C units present in the backbone. There was a slight increase in the intensities of CH_2 stretching peaks at 2945 and 2882 cm^{-1} .

However, the most significant changes were detected in 1300 to 700 cm^{-1} region. Figure 3.9. and Figure 3.10. give the the 1300-1000 cm^{-1} and 1000-700 cm^{-1} regions of the FTIR spectra for PEO-2000 mixtures with different loadings of hydrophobic (HDK H2K) and hydrophilic (HDK N20) silica respectively. In literature, it is mentioned that the peaks at

1282 and 1242 cm^{-1} correspond to the asymmetric CH_2 twisting modes of the poly(ethylene oxide) backbone [39, 40, 41]. As can be seen in Figures 3.3. and 3.4, upon incorporation of any type of silica intensities of these peaks diminished, indicating an interaction between silica nanoparticles and the oligomer chains.

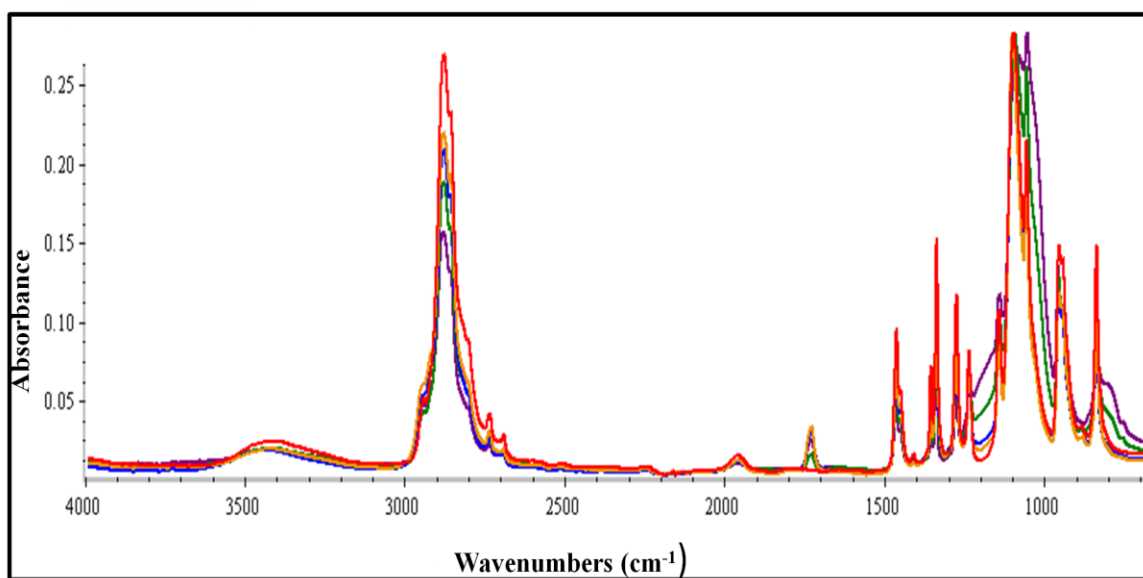
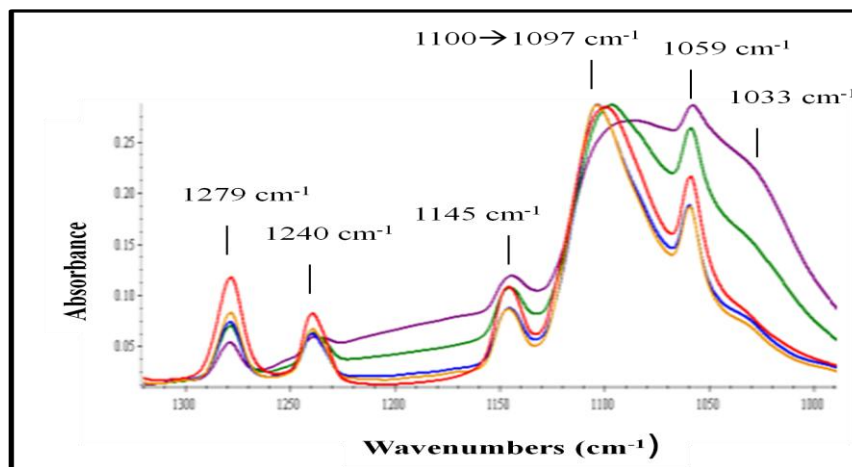
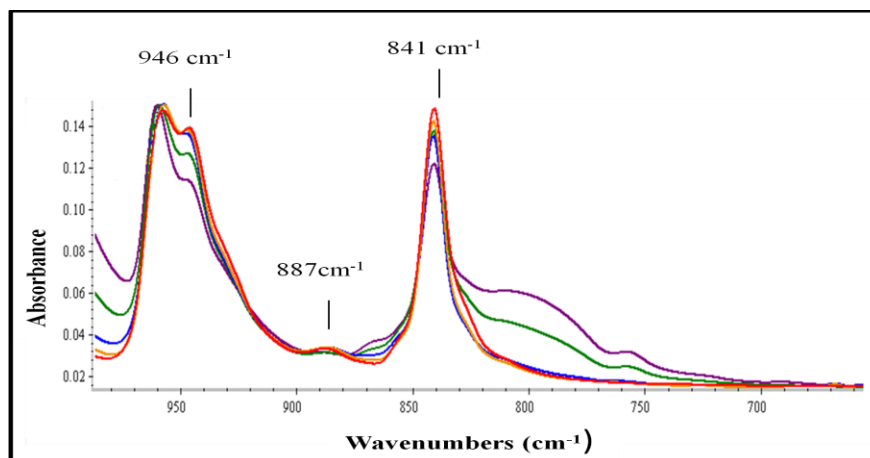


Figure 3.8. FTIR-IR spectra of PEO2000 and mixtures with various loadings of HDK H2K: red (neat), orange (1%), blue (5%), green (10%), and purple (20%)

The peaks at 1145, 1100, and 1059 cm^{-1} correspond to the C-O-C stretching modes of poly(ethylene oxide) backbone. As can be seen from the spectra provided in Figures 3.9.A. and 3.10.B. upon either type of fumed silica addition, especially the peak at 1100 shifted to lower wavenumbers. Shift to lower wavenumbers was an indication of an increase in H-bonding. The intensity of the peaks at 1100 and 1059 cm^{-1} increases also since Si-O stretching peaks overlap with C-O-C stretching peaks of poly(ethylene oxide) oligomer.

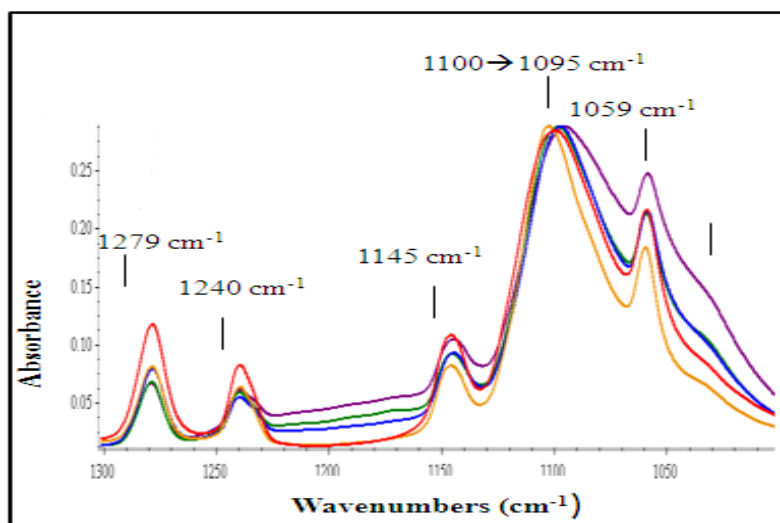


(A)

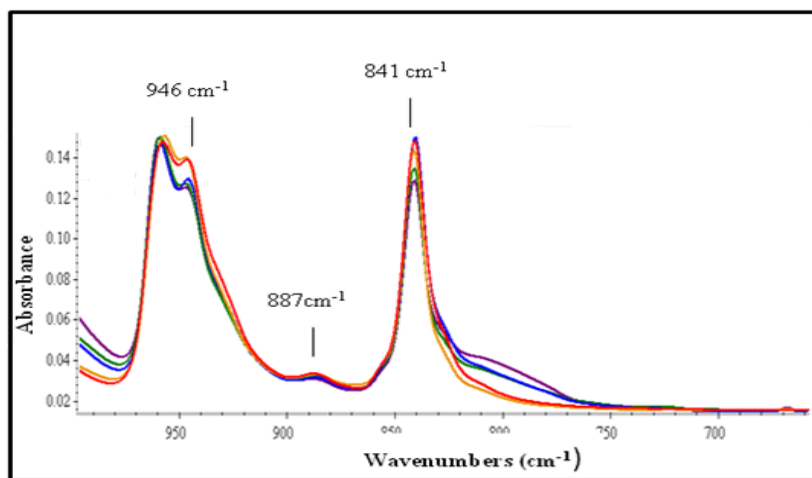


(B)

Figure 3.9. (A) 1300-1000 cm^{-1} and (B) 1000-700 cm^{-1} regions of model PEO-2000 mixtures with various loadings of HDK H2K: red (neat), orange (1%), blue (5%), green (10%) and purple (20%)



(A)



(B)

Figure 3.10. (A) 1300-1000 cm^{-1} and (B) 1000-700 cm^{-1} regions of the FTIR spectra for PEO-2000 mixtures with various loadings of HDK N20: red (neat), orange (1%), blue (5%), green (10%) and purple (20%)

As can be seen in Figures 3.9.B. and 3.10.B. the peaks in $1000\text{-}700\text{ cm}^{-1}$ region also showed dramatic changes. According to literature, the peaks in this region are the asymmetric CH_2 rocking modes of the poly(ethylene oxide) backbone and they give information about the helical turns of the poly(ethylene oxide) oligomers and thus about its crystallinity [39, 40, 41, 42]. The peaks at 946 and 841 cm^{-1} represent the rocking vibrations of $\text{CH}_2\text{-CH}_2$ in gauche form, which are schematically shown in Figure 3.11., and account for the crystallinity of the chains also, whereas the peak at 887 cm^{-1} represents the rocking vibrations of O-CH_2 in trans form. A decrease in the intensity of the peaks at 946 and 841 cm^{-1} upon both types of fumed silica addition was an indication of a change in the helical conformation of the poly(ethylene oxide) oligomers meaning a decrease in crystallinity. Another interesting observation in the ATR-IR studies, shown in Figure 3.12., was the appearance of a small peak around 1730 cm^{-1} upon silica addition, which was not present in the pure oligomer. This additional peak may also indicate presence of interactions between fumed silica and PEO oligomers.

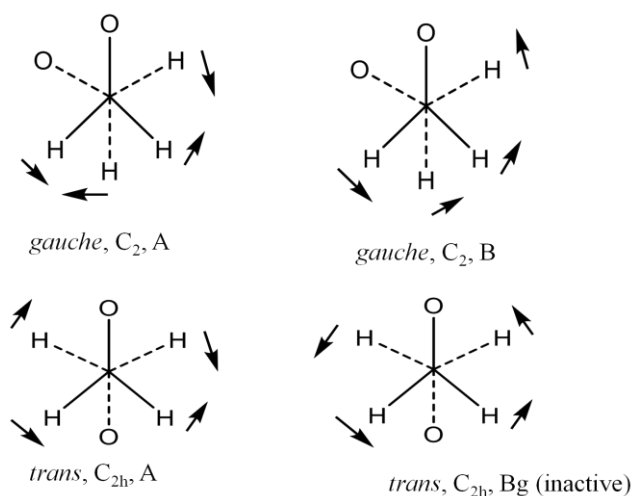


Figure 3.11. Schematic representations of gauche and trans forms in poly(ethylene oxide) chains [40].

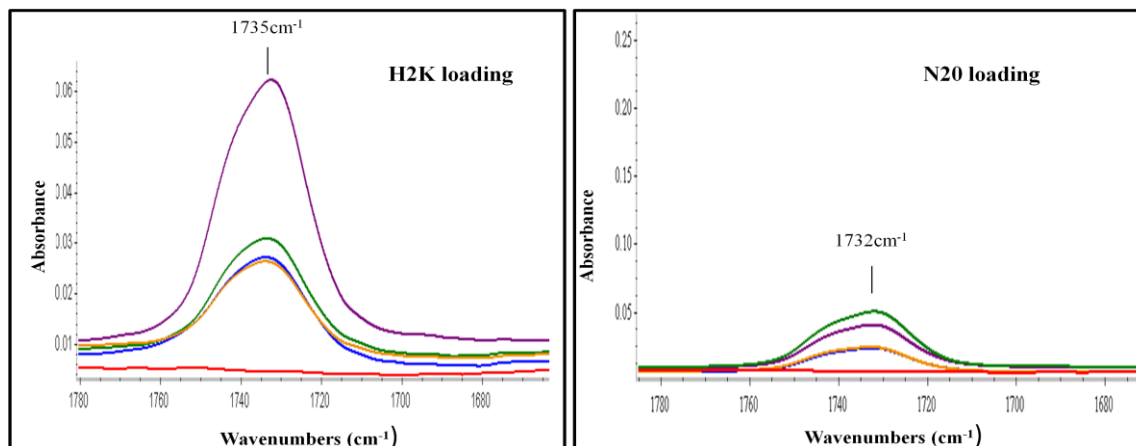


Figure 3.12. 1780-1680 cm⁻¹ region of the FTIR spectra for PEO-2000 mixtures with HDK H2K (left) and HDK N20 (right) loadings: red (neat), orange (1%), blue (5%), green (10%), purple (20%)

3.2.1.3. ATR-IR Investigation of Poly(tetramethylene oxide) PTMO-2000 and Fumed Silica Mixtures

FTIR-IR spectra of PTMO-2000 and its mixtures with various loadings of HDK H2K are reproduced in Figure 3.13. Spectra obtained from both air and mold sides of the samples were identical indicating an even distribution of fumed silica particles throughout the PTMO oligomers. Similar to the observations made in PEO mixtures the hydroxyl peak of PTMO oligomer was not affected upon addition of either hydrophilic or hydrophobic fumed silica. The symmetric and asymmetric CH₂ stretching peaks at 3000 to 2600 cm⁻¹ region were not affected by the fumed silica addition, which was different when compared to the results observed in PEO-2000-fumed silica mixtures.

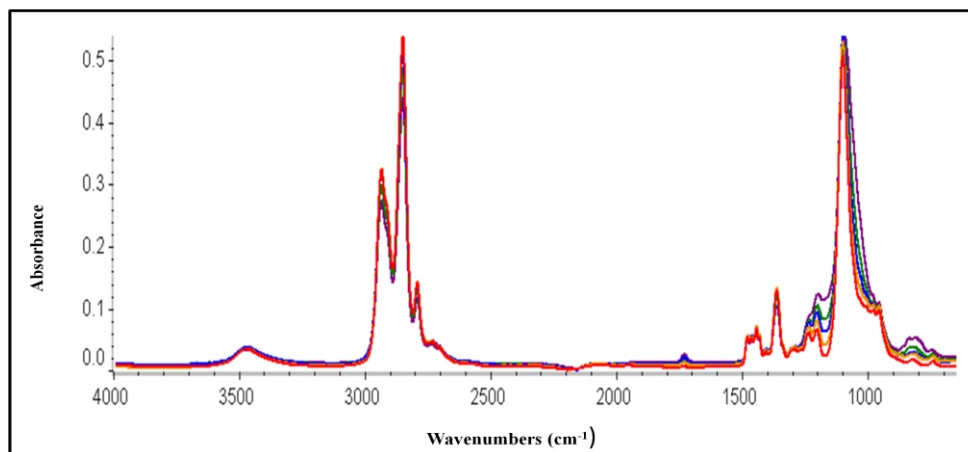


Figure 3.13. FTIR spectra of PTMO-2000 mixtures with various loadings of HDK H2K: red (neat), orange (1%), blue (5%), green (10%) and purple (20%)

As shown in Figure 3.14 appearance of a very small peak at 1730 cm^{-1} was observed in poly(tetramethylene oxide)/fumed silica mixtures, but only in case of hydrophobic silica addition. We are not very sure about the origins of this rather weak absorption peak.

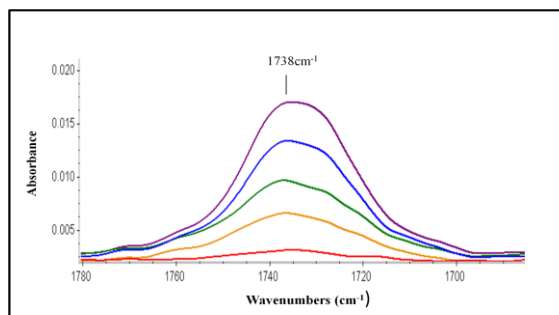


Figure 3.14. $1780\text{-}1680\text{ cm}^{-1}$ region of the FTIR spectra for PTMO-2000 mixtures with various HDK H2K loadings: red (neat), orange (1%), blue (5%), green (10%) purple (20%)

There was a significant difference in the spectra of mixtures and pure oligomer in 1300 to 700 cm^{-1} region (Figures 3.15. and 3.16). The intensity of the CH_2 twisting peaks at 1242 and 1210 cm^{-1} increased. The peak at 1102 cm^{-1} and the shoulder at 1060 cm^{-1} had an increase in intensity and they shift to lower wavenumbers indicating that new H-bonds upon fumed silica incorporation and coincidence of C-O-C and Si-O stretching peaks. However, the shifts were not as pronounced as the shifts of poly(ethylene oxide) based models due to less number of ether units in the oligomer backbone. The intensity of the peak at 950 cm^{-1} decreased in blends gradually whereas intensities of the small peaks at 850 to 800 cm^{-1} increased which may be the result of a change oligomer alignment.

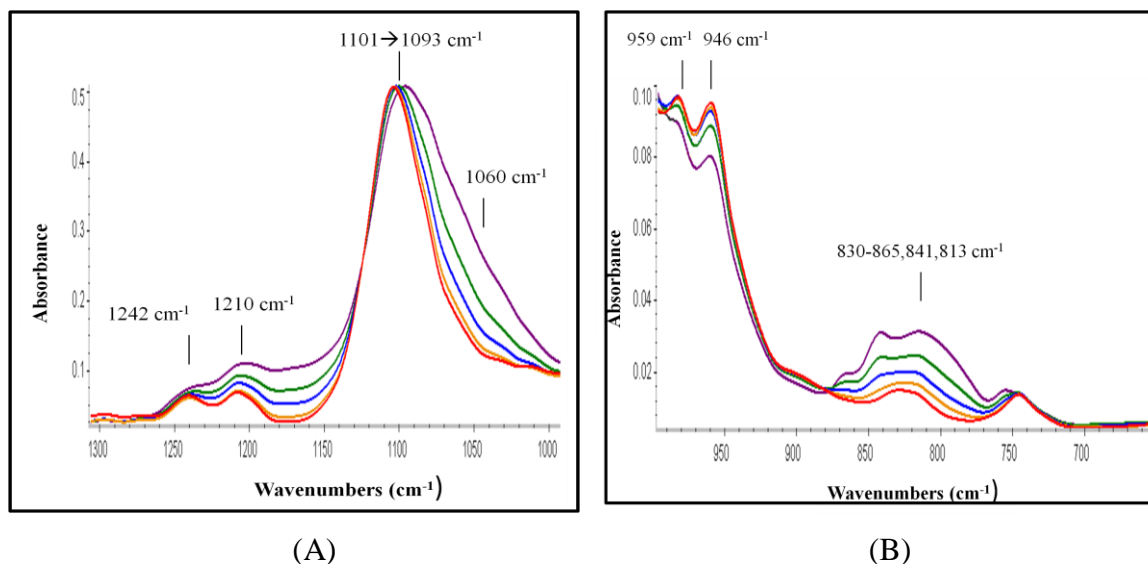
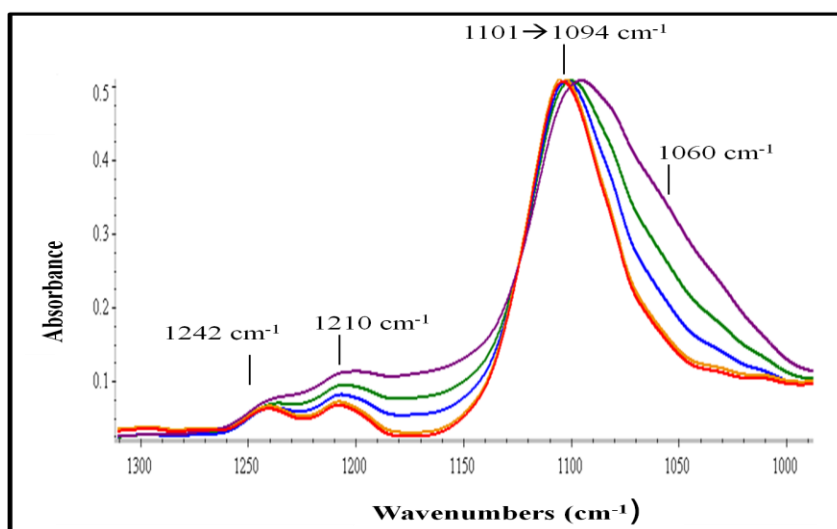
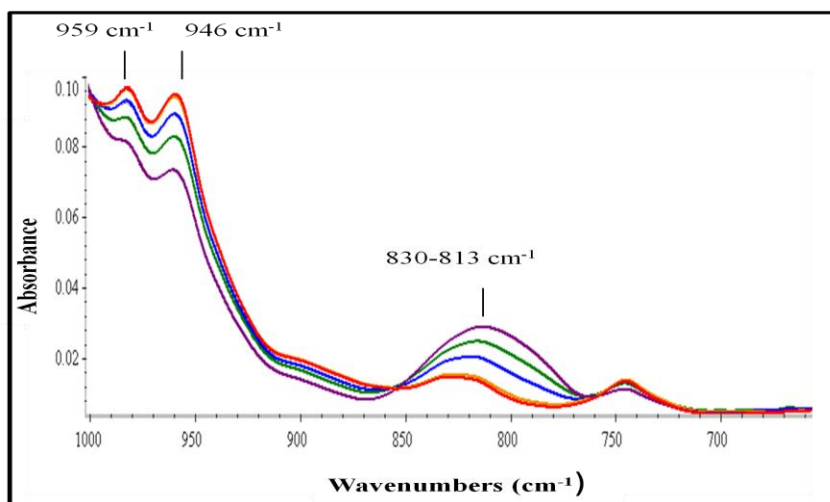


Figure 3.15. (A) 1300-1000 cm^{-1} and (B) 1000-700 cm^{-1} regions of PTMO-2000 mixtures with various loadings: red (neat), orange (1% HDK H2K), blue (5% HDK H2K), green (10% HDK H2K), and purple (20% HDK H2K)



(A)



(B)

Figure 3.16. (A) 1300-1000 cm^{-1} and (B) 1000-700 cm^{-1} regions of the FTIR spectra for PTMO-2000 mixtures with various loadings of HDK N20: red (neat), orange (1%), blue (5%), green (10%) and purple (20%)

3.2.2. FTIR and ATR-IR Investigation of PEO2-UU30 based Nanocomposites

In FTIR spectra of polyurethanes and polyurethaneureas, the peaks in 3500 and 3250 cm^{-1} range represent free and H-bonded N-H vibrations, whereas the peaks between 1750 and 1650 cm^{-1} represent free and H-bonded urethane and urea carbonyl stretching vibrations [43]. Additionally, the peaks between 3000 and 2600 cm^{-1} region are for CH_2 stretching peaks of the same polymers. As a result, in this part of our investigations we focused mainly on these regions of the FTIR spectra. Position and appearance of some of these peaks were changed by fumed silica incorporation into the polymer matrix indicating differences in H-bonding characteristics of the composites, compared to neat polyurethanes.

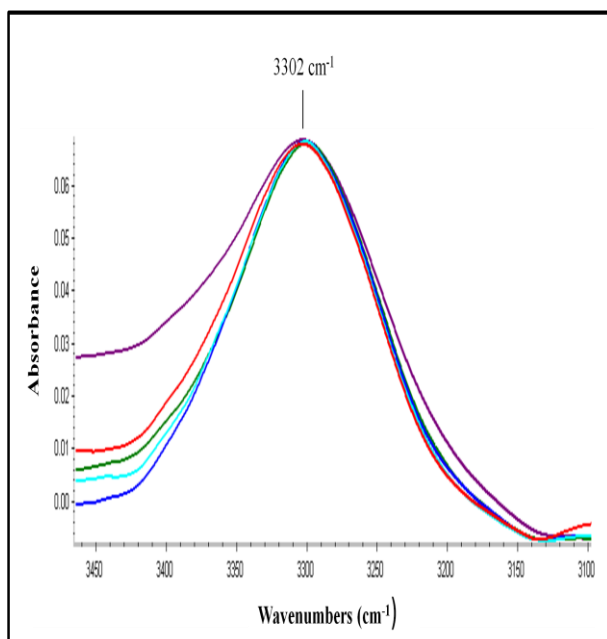
Results obtained from ATR-IR spectra of the polymers and nanocomposites are similar to the results inferred from FTIR spectra. In case of ATR-IR spectra, however, the peak shifts at urethane carbonyl region and polyether region could be detected more precisely since these less polar units are more close to the surface than the highly polar urea groups. Therefore, the appearance of a freshly formed peak at 1745 cm^{-1} corresponding to the non-bonded urethane carbonyl at high fumed silica loadings could only be detected from the ATR-IR spectra of the nanocomposites.

3.2.2.1. FTIR studies on PEO2-UU30 based Nanocomposites

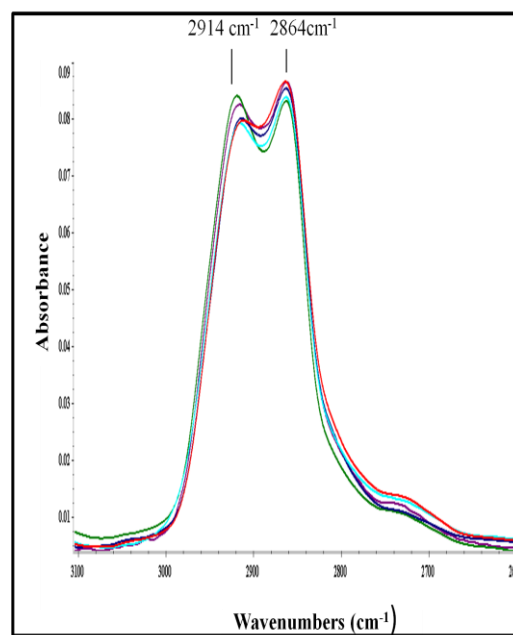
Different regions of the FTIR spectra for neat polymer and nanocomposites containing different amounts of hydrophobic silica H2K are reproduced in Figure 3.17. A-D. As reproduced on Figure 3.17.A, no noticeable difference could be detected in the N-H regions

of the neat polymer and nanocomposites in case of both HDK H2K and HDK N20 addition. Similarly the CH₂ stretching vibrations changed only slightly upon fumed silica incorporation as shown on Figure 3.17. B. The peak at 2917 cm⁻¹ increased in intensity, whereas the peak at 2862 cm⁻¹ decreased in intensity gradually with fumed silica addition. This change may be the result of some conformational changes in the polymer chains in the nanocomposite.

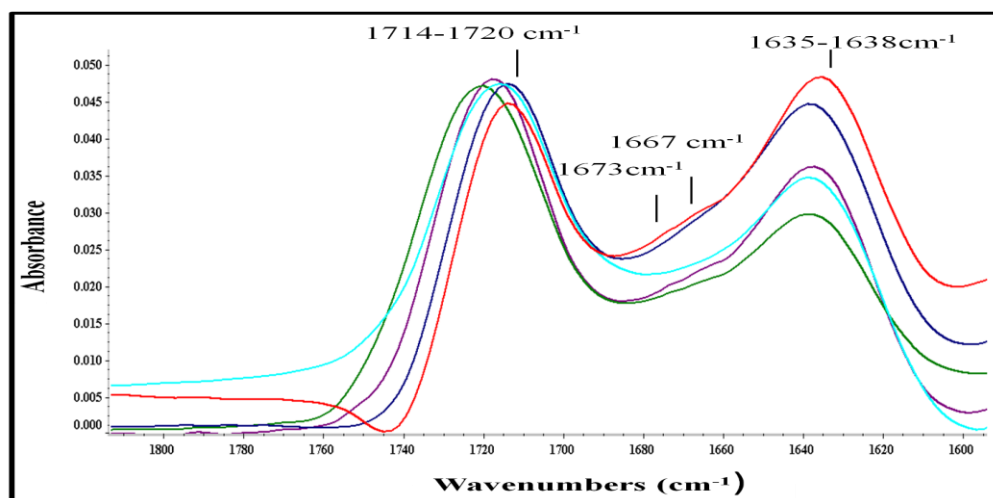
As can be seen in Figure 3.17.C. two peaks and a shoulder is observed in the carbonyl region. In both types of fumed silica incorporation, the peak at 1715 cm⁻¹ due to the disordered H-bonded urethane carbonyl groups shifted to higher wavenumbers meaning a decrease in H-bonding of urethane units. The peak at 1635 cm⁻¹ corresponding to the ordered H-bonded urea carbonyls decreased in intensity and shifted to higher wavenumbers slightly, which also indicated that both types of fumed silica addition change and disrupt the H-bonding of carbonyl region. As provided in Figure 3.17. D. the absorption peaks at 1139, 1109, and 1041 cm⁻¹ correspond to the C-O-C stretching modes of the polyether backbone. It was observed that upon fumed silica addition, in general all of the peaks grew in intensity and the peaks at 1109 and 1041 cm⁻¹ shifted to lower wavenumber indicating an increase in H-bonding interaction between the ether and the urethane or urea groups in the hard segments. Increase in intensity can be explained as overlapping of Si-O stretching peaks with C-O-C stretching peaks of the polymer. However, the peak at 1350 cm⁻¹ for CH₂ wagging vibration decreased in intensity, which may be an indication of a change in the chain conformation. It was inferred from the spectral observations that fumed silica slightly disrupted the hydrogen bonding between the hard segments in the polymer matrix and also interacted with the ether units in the soft segments. Interestingly, both hydrophilic and hydrophobic fumed silica additions caused similar changes on the spectra.



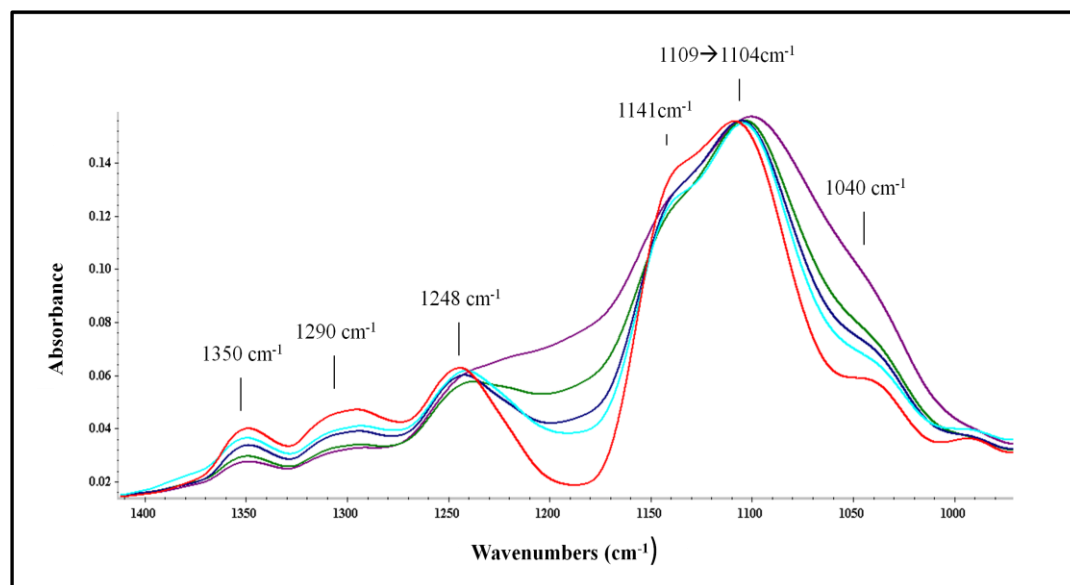
(A)



(B)



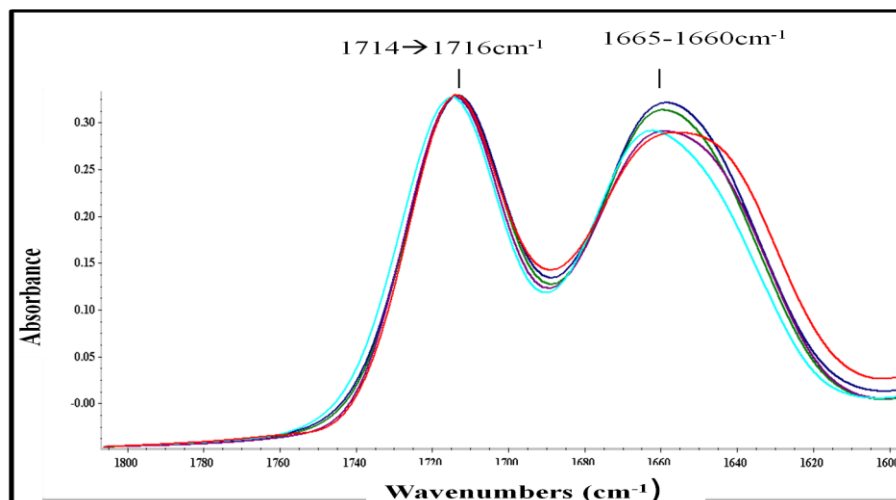
(C)



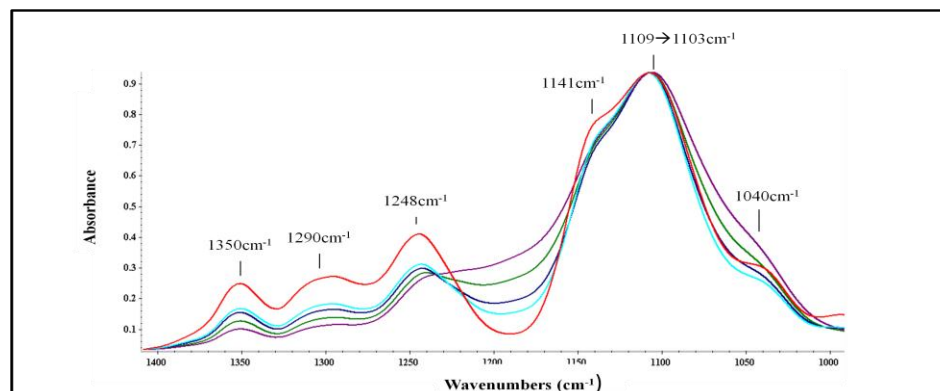
(D)

Figure 3.17. Various regions of the FTIR spectra of PEO2-UU30 and corresponding nanocomposites containing HDK H2K. (A) 3500-3100 cm^{-1} (B) 3100-2600 cm^{-1} , (C) 1800-1600 cm^{-1} , and (D) 1400-1000 cm^{-1} regions: red (neat), light blue (5%), blue (10%), green (20%), purple (40%)

Figures 3.18.A and 3.18.B. provide the carbonyl region (1800-1600 cm^{-1}) and ether region (1400-1000 cm^{-1}) of the FTIR spectra of virgin PEO2-UU30 copolymer and its nanocomposites with hydrophilic silica HDK N20. As can be seen from the spectra in Figures 3.18.A. and 3.18.B. very similar interaction behavior was observed in hydrophilic HDK N20 containing nanocomposites as that of hydrophobic HDK H2K systems with the base PEO2-UU30 polyurethaneurea.



(A)



(B)

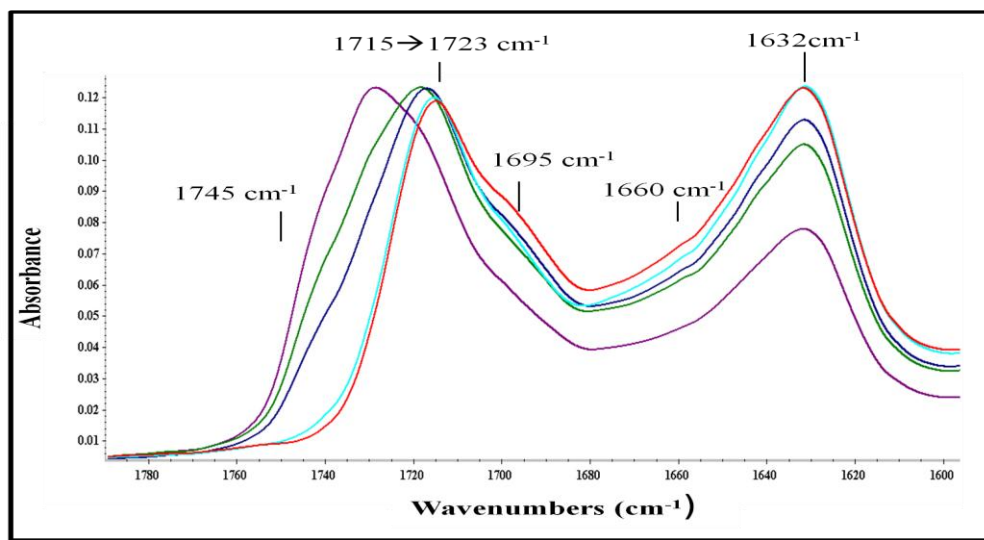
Figure 3.18. Various regions of the FTIR spectra of PEO2-UU30 and corresponding nanocomposites containing HDK N20. (A) 1800-1600 cm^{-1} , and (B) 1400-1000 cm^{-1} regions: red (neat), light blue (5%), blue (10%), green (20%), purple (40%)

3.2.2.2. ATR-IR studies on PEO2-UU30 based Nanocomposites

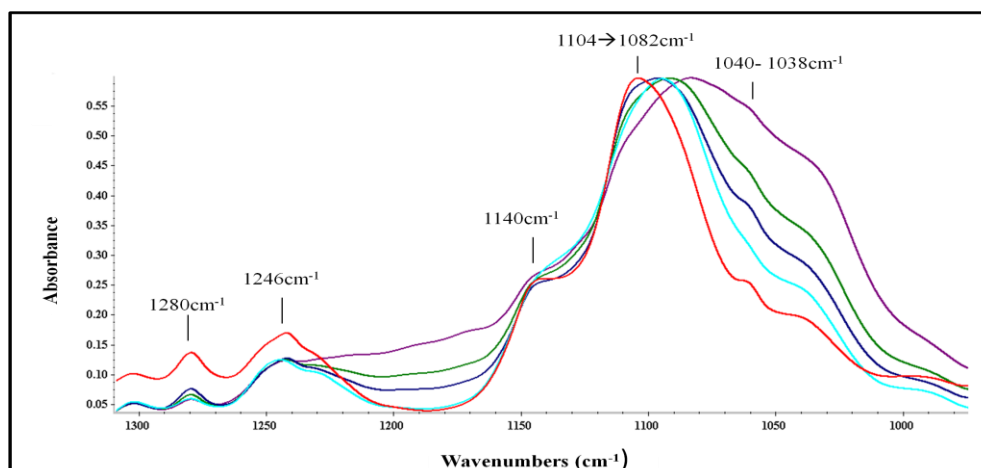
As already briefly mentioned previously, ATR-FTIR spectra which is surface sensitive seem to provide better peak resolution in nanocomposites the in both carbonyl and also ether regions as shown in Figures 3.19. (H2K filled nanocomposites) and 3.20. (N20 filled nanocomposites).

Comparative ATR spectra for the carbonyl region of H2K containing nanocomposites are provided Figure 3.19.A. As can be seen from this figure, the shift to higher wavenumbers of the disordered H-bonded urethane carbonyl peak is more pronounced. Additionally, at high fumed silica loadings (10-40 wt %) a freshly formed peak is observed at 1745 cm^{-1} which is attributed to non-bonded urethane carbonyls proving again that filler incorporation disrupts the H-bonding pattern of the hard segment domains. Moreover, diminishing in intensity of the urea carbonyl peak is also observed in the ATR-IR spectra of PEO2-UU30 and corresponding composites.

As shown in Figure 3.19.B., the polyether region of PEO2-UU30 and H2K filled nanocomposites can be analysed in a more detailed fashion with ATR-IR. Shift of the C-O-C stretching peak at 1109 cm^{-1} and also broadening of the same peak is more dramatic in the ATR-IR spectra indicating new H-bonds formed between the fumed silica surface and oxygen of the polyether region. Broadening of the peaks at 1141 and 1109 cm^{-1} is also more pronounced in the ATR-IR spectra. Similar to our findings from the FTIR studies, type of fumed silica incorporated (hydrophobic or hydrophilic) does not affect the interaction with the matrix significantly.

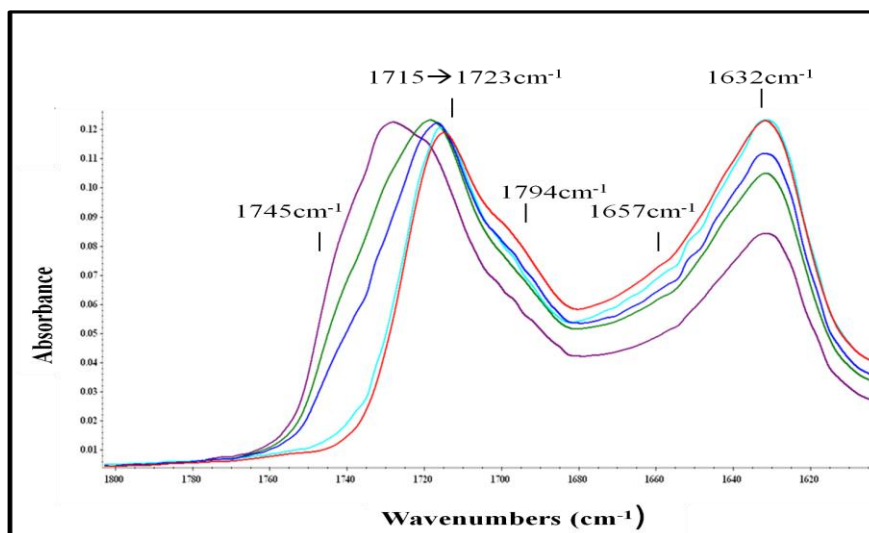


(A)

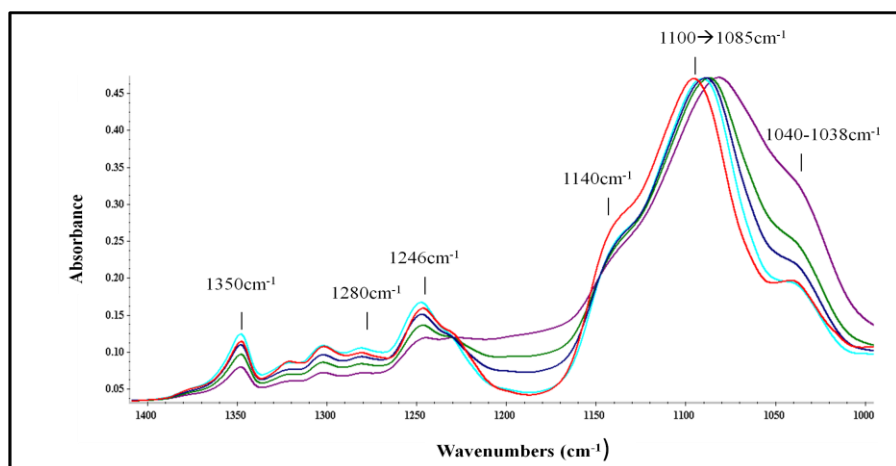


(B)

Figure 3.19. ATR-IR spectra of PEO2-UU30 and its nanocomposites with HDK H2K (A) 1800-1600 cm^{-1} , and (B) 1300-1000 cm^{-1} regions: red (neat), light blue (5%), blue (10%), green (20%), purple (40%)



(A)



(B)

Figure 3.20. ATR-IR spectra of PEO2-UU30 and its nanocomposites with HDK N20 (A) 1800-1600 cm^{-1} , and (B) 1300-1000 cm^{-1} regions: red (neat), light blue (5%), blue (10%), green (20%), purple (40%)

3.2.3.1. FTIR Spectra of PTMO2-UU20 based Nanocomposites

Different regions of the FTIR spectra for PTMO2-UU20 copolymer and its nanocomposites containing different amounts of hydrophobic silica H2K are reproduced in Figure 3.21. A-D. As can be seen in Figure 3.21.A, no noticeable differences could be detected in the N-H regions of the neat polymer and nanocomposites upon the incorporation of HDK H2K into the polymer. This is similar to our observations in PEO2-UU30 based nanocomposites. As shown in Figure 3.21.B., the CH₂ stretching vibrations of the polymer at 3100 to 2600 cm⁻¹ region were also not affected by fumed silica addition meaning that silica addition did not affect the chain conformation as much as in case of poly(ethylene oxide) based polyurethaneureas. Interestingly we could not observe any significant difference in the carbonyl region (1800-1600 cm⁻¹) of the FTIR spectra between the host copolymer and the H2K containing nanocomposites, as shown in Figure 3.21.C. Two major absorption peaks in the carbonyl region are centered at 1717 and 1637 cm⁻¹ in the spectrum indicating the disordered H-bonded urethane and ordered, H-bonded urea groups of the polymer, respectively. Very slight shifts to the higher wavenumbers were seen in that region upon hydrophobic fumed silica incorporation with a slight decrease in intensity of the urea peak. Almost the same trend was observed in the carbonyl region of the neat polymer and corresponding nanocomposites after hydrophilic fumed silica addition, as shown in Figure 3.22.A.

The peaks at 1111 and 1043 cm⁻¹ correspond to the C-O-C stretching modes. Both hydrophilic and hydrophobic fumed silica addition caused these peaks to broaden due to overlapping of Si-O and C-O stretching peaks. However, no dramatic differences in peak positions were detected upon fumed silica incorporation in FT-IR spectra.

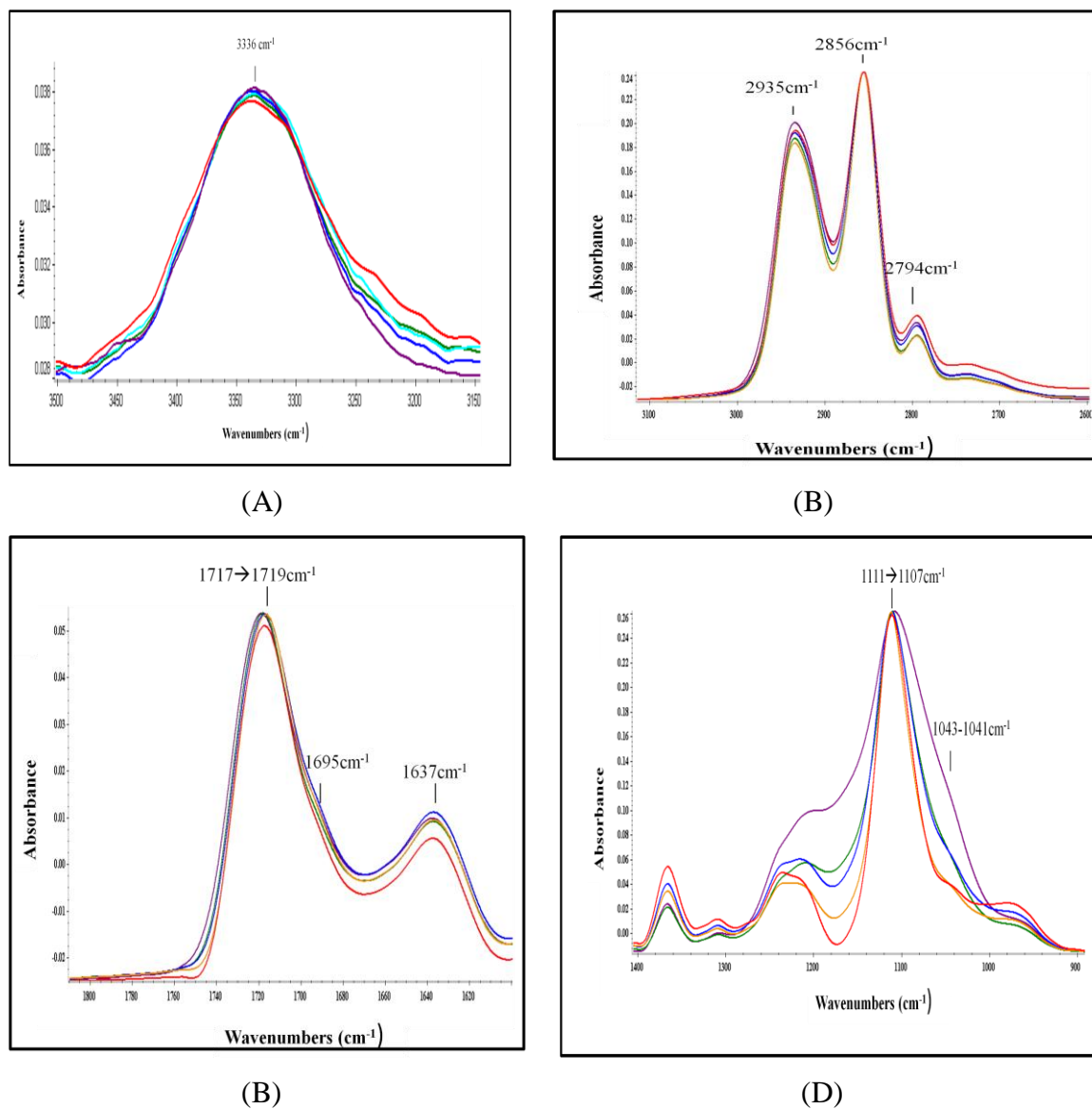
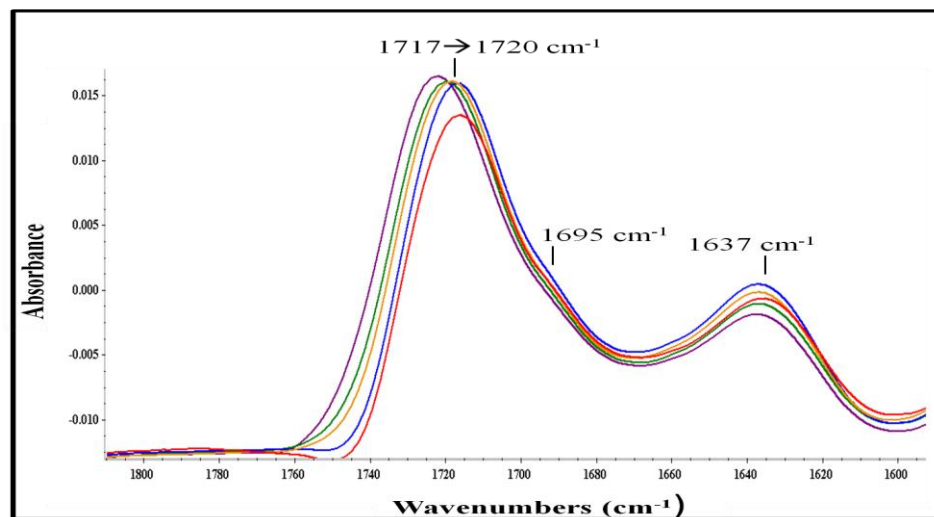
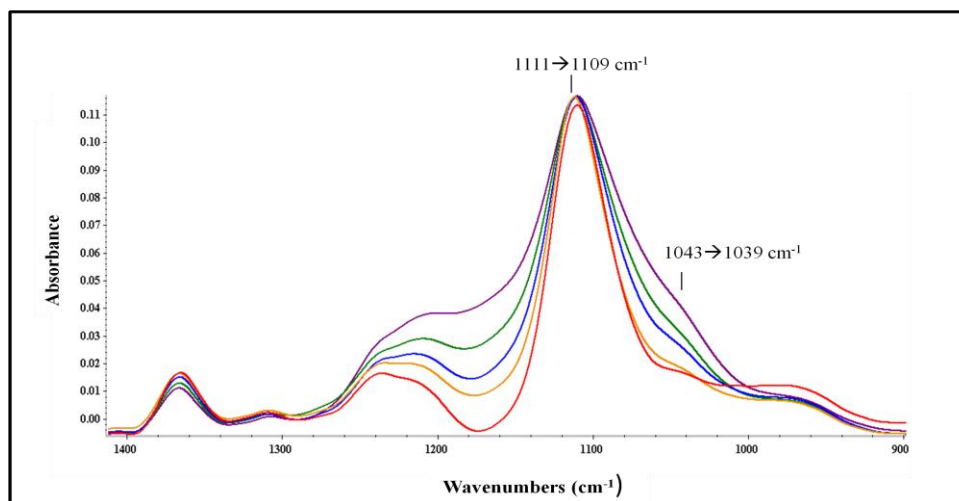


Figure 3.21. FT-IR spectra of PTMO2-UU20 and corresponding nanocomposites containing HDK H2K. (A) 3500-3100 cm^{-1} (B) 3100-2600 cm^{-1} , (C) 1800-1600 cm^{-1} , and (D) 1400-900 cm^{-1} regions: red (neat), light blue (5%), blue (10%), green (20%), purple (40%)



(A)



(B)

Figure 3.22. FT-IR spectra of PTMO2-UU20 and corresponding nanocomposites containing HDK N20. (A) 1800-1600 cm^{-1} and (B) 1400-900 cm^{-1} regions: red (neat), orange (5%), blue (10%), green (20%), purple (40%)

3.2.3.2. ATR-IR Spectra of PTMO2-UU20 based Nanocomposites

Similar to that of PEO2-UU30 based systems, results obtained from ATR-IR spectra of the same polymers and nanocomposites similar to the results inferred from FT-IR spectra. As shown in Figures 3.22.A and 3.23.A., carbonyl region of the neat polymer and the corresponding nanocomposites could be observed in more detail. In Figures 3.22.B. and 3.23.B. it can be seen that ATR-IR spectra of the polymer and nanocomposites reveal also much more intense shifts in the 1300-1000 cm^{-1} region. Shifts to lower wavenumbers due to H-bonding between silica silanol groups and ether units in the polymeric backbone were detected in ATR-IR spectra of the same nanocomposites. The studies based on FTIR and ATR-IR indicated that longer ether units in the soft segment backbone as in PTMO based polyurethaneureas seem to lead to less interaction of filler and polymer soft segment.

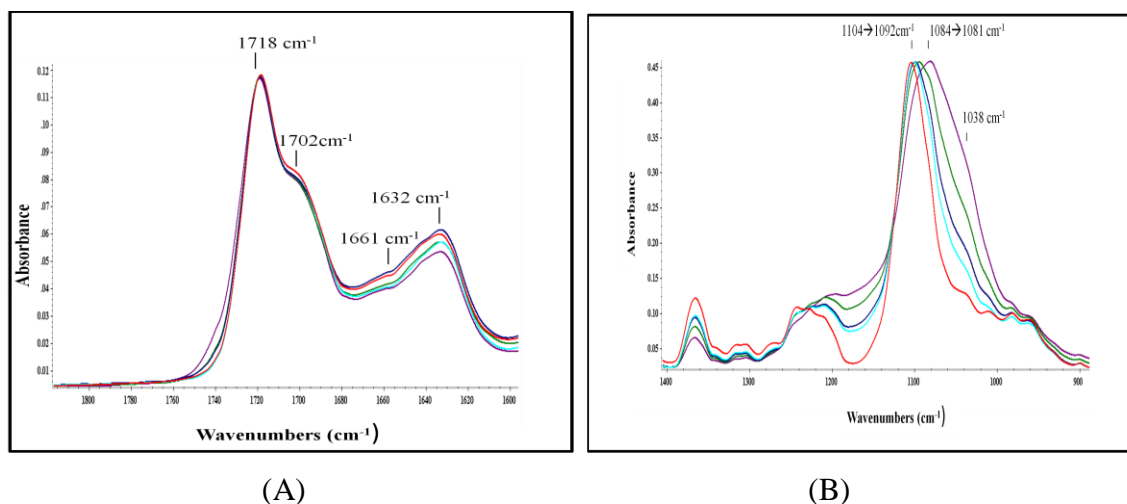
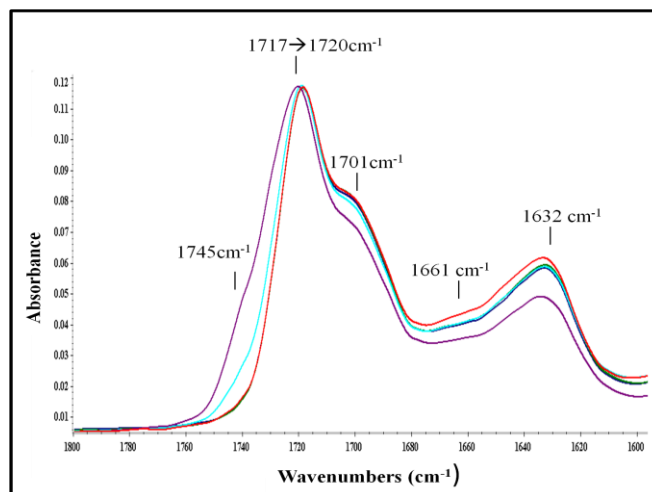
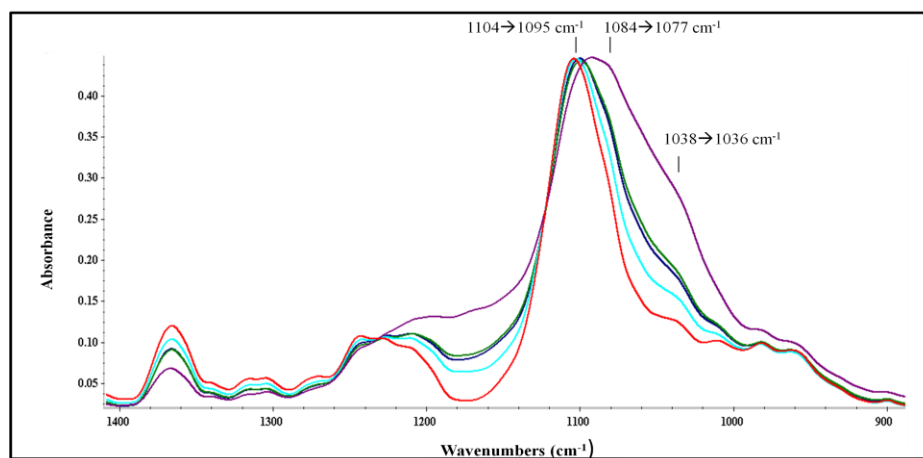


Figure 3.23. ATR-IR spectra of neat polymer and corresponding nanocomposites. (A) 1800-1600 cm^{-1} , and (B) 1400-900 cm^{-1} regions: red (neat), light blue (5% HDK H2K), blue (10% HDK H2K), green (20% HDK H2K), purple (40% HDK H2K)



(A)



(B)

Figure 3.24. ATR-IR spectra of PTMO2-UU20 and corresponding nanocomposites. (A) 1800-1600 cm⁻¹, and (B) 1400-900 cm⁻¹ regions: red (neat), light blue (5% HDK N20), blue (10% HDK N20), green (20% HDK N20), purple (40% HDK N20)

3.2.4. Silicone- urea based Nanocomposites

N-H peak at 3300-3400 cm^{-1} region and CH_2 stretching peaks at 2800-3000 cm^{-1} region of silicone-urea based polymers were not affected by fumed silica incorporation to the matrix. There were two stretching peaks, amide I and amide II in the urea carbonyl stretching region at 1633 and 1566 cm^{-1} , respectively. These peaks did not reveal a change upon hydrophobic silica incorporation meaning that fumed silica addition did not disturb the H-bonding capability of the hard segments. The peak at 1261 cm^{-1} was due to the CH_3 stretching vibrations attached to the Si atoms along the backbone. The doublet at 1095 and 1022 cm^{-1} correspond to the Si-O stretching vibrations of the PDMS backbone and they were broadened upon silica incorporation due to overlapping of fumed silica Si-O bonds with those of PDMS chain. The intensity of the peak at 1094 cm^{-1} increased in intensity whereas intensity of the peak at 1022 cm^{-1} decreased in nanocomposites indicating an interaction between fumed silica and the polymer matrix. ATR-IR spectra revealed the same results about nanocomposites and therefore are not shown here.

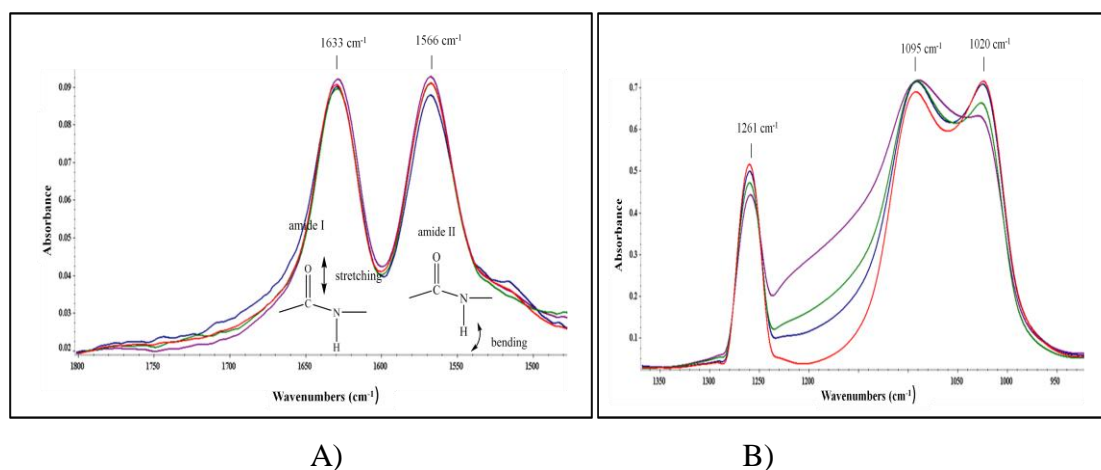


Figure 3.25. FT-IR spectra of neat polymer and corresponding nanocomposites in (A) 1800-1500 cm^{-1} , (B) 1400-900 cm^{-1} regions: red (neat), light blue (5% HDK H2K), blue (10% HDK H2K), green (20% HDK H2K), purple (40% HDK H2K)

3.3. The DSC Studies of the Oligomers

DSC results of neat PEO-2K, PTMO-2K and PDMS-32K oligomers and the model mixtures prepared from these oligomers containing 10% by weight of both hydrophilic and hydrophobic fumed silica are given in Table 3.6. The glass transition temperatures of neat and fumed silica filled PEO-2K oligomers could not be determined because of their high crystallinity the change in heat capacity of these systems was below the sensitivity limits of the DSC instrument used. As shown on Table 3.6. the melting points of the H2K and N20 filled oligomers (55.5 and 54.8 °C respectively) were slightly lower than that of the pure PEO-2K, indicating that all had similar crystal structures. However, as can also be seen on Table 3.6., a significant drop from 607 to 127 and 118 J/g in the heat of fusion value was detected for 10% H2K and 10% N20 mixtures respectively, when compared with neat PEO-2K. These results indicate that upon incorporation of either type of silica, crystallinity of PEO-2K was reduced by about 80%. Such a sharp drop in the heat of fusion values may indicate that both hydrophobic and hydrophilic fumed silica reduced the packing capability of the poly(ethylene oxide) oligomer chains.

Table 3.6. DSC Results of the oligomers and mixtures.

	T_g (°C)	ΔC_p (J/gK)	T_m (°C)	ΔH_f (J/g)
PEO2K	-	-	59.2	607.4
PEO2K/10wt%HDK H2K	-	-	55.5	127
PEO2K/10wt%HDK N20	-	-	54.8	118
PTMO2K	-	-	30.6	273.5
PTMO2K/10wt%HDK H2K	-	-	27.2	72.65
PTMO2K/10wt%HDK N20	-	-	27.7	73.77
PDMS32K	-125.1	0.287	-	-
PDMS32K/10wt%HDK H2K	-125	0.086	-	-

As can be seen from Table 3.6., very similar results were obtained for PTMO-2K based model mixtures in terms of the reduction in total crystallinity upon silica incorporation. These findings show that the changes in packing behavior of polyether soft segments in nanocomposites indicated by the ATR-IR studies were in line with the DSC results.

The glass transition temperature of polydimethylsiloxane oligomer was not influenced after hydrophobic fumed silica H2K addition. But about 30% reduction in the specific heat capacity compared to pure oligomer clearly indicated immobilization of the PDMS oligomer chains due to interaction with the fumed silica incorporated.

3.4. Optical Microscopy Studies of Model Compounds

1,3-Dimethylurea (DMU) and its mixtures with 10 wt% HDK H2K, and 10 wt% HDK N20 were prepared in THF. The solution and the corresponding mixtures were dropcast onto glass slides and left at room temperature for 24 hours for the complete evaporation of the THF solvent. During this process the systems also crystallized. The optical microscopy (OM) images of the samples were taken at room temperature. As already discussed earlier, DMU was used to mimic the urea hard segments in polyurethanes and the model compounds prepared by fumed silica addition were used in order to investigate the effect of fumed silica addition on the crystallization behaviour of the hard segments. These images are shown in Figure 3.26.

As can be seen in the OM images provided in Figure 3.26. both hydrophobic and hydrophilic fumed silica additions affected the crystallization behavior and crystal structure of DMU to some extent. From these results it can be concluded that fairly strong interaction exists between the silica fillers and the urea hard segments in the copolymers.

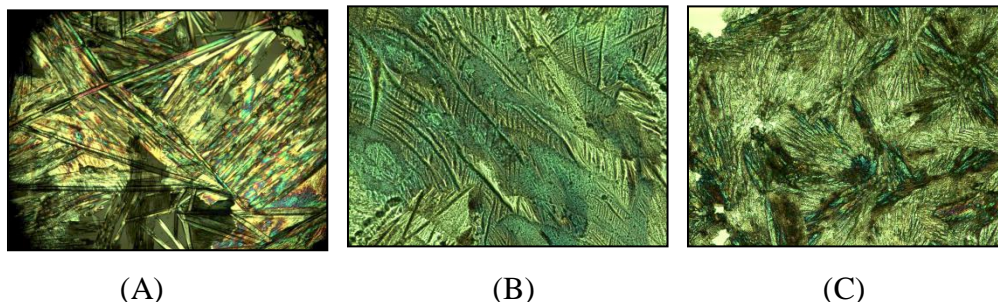


Figure 3.26. Polarized OM images of (A) 1,3-dimethylurea, (B) 1,3-Dimethylurea/10 wt % HDK H2K, and (C) 1,3-Dimethylurea/HDK N20 with 10X magnification at RT

This conclusion was also supported by the WAXD patterns of the neat polymers and polymer-fumed silica nanocomposites where the hard segment peaks have diminished after fumed silica addition. Reduced H-bonding between hard segments evidenced by carbonyl peak shifts in the FTIR and ATR-IR spectra was another indication of fumed silica interaction with the urea hard segments.

3.5. X-Ray Diffraction (XRD) Studies

XRD is commonly used in the characterization of polymeric nanocomposites containing inorganic fillers, such as organoclay, silica, etc. It provides detailed information on the extent of organoclay dispersion or intercalation through the use of the Bragg's Law:

$$\sin\theta = n\lambda/2d$$

where d is the spacing between the atomic planes in the crystalline phase and λ is the X-Ray wavelength. The intensity is measured as a function of the diffraction angle 2θ and the specimen's orientation. This diffraction pattern is used to identify the specimen's crystalline phases and to measure its structural properties. Because of being nondestructive and not needing elaborate sample preparation, XRD is a widely used technique [20]. Although fumed silica is amorphous and does not show sharp peaks in the XRD experiments. But, as shown in Figure 3.27. it has a broad peak at $2\theta = 22^\circ$ irrespective of being hydrophobic or hydrophilic. This result is also consistent with the literature [44, 45, 46].

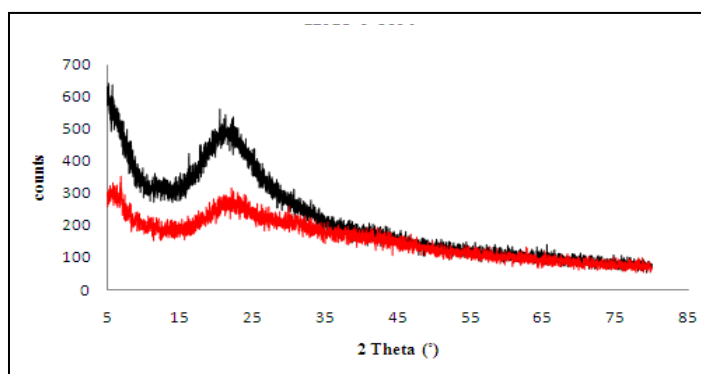


Figure 3.27. XRD patterns of hydrophilic HDK N20 (red) and hydrophobic HDK H2K (black)

On the other hand as shown in Figure 3.28. PEO-2K oligomer shows two intense peaks at $2\theta = 20^\circ$ and $2\theta = 25^\circ$ and additional peaks at $2\theta = 15^\circ$, $2\theta = 23.5^\circ$, $2\theta = 27^\circ$ and $2\theta = 36^\circ$ because of the semi-crystalline nature of PEO-2K oligomers. On the other hand PEO2-UU30 copolymer shows two broad peaks at $2\theta = 20^\circ$ and $2\theta = 25^\circ$ with a broad shoulder at $2\theta = 9^\circ$ indicating partially crystalline nature of the polymer matrix.

As can be seen in Figure 3.29 and Figure 3.30. incorporation of either hydrophilic or hydrophobic fumed silica dramatically changes the XRD patterns of PEO-2K blends and

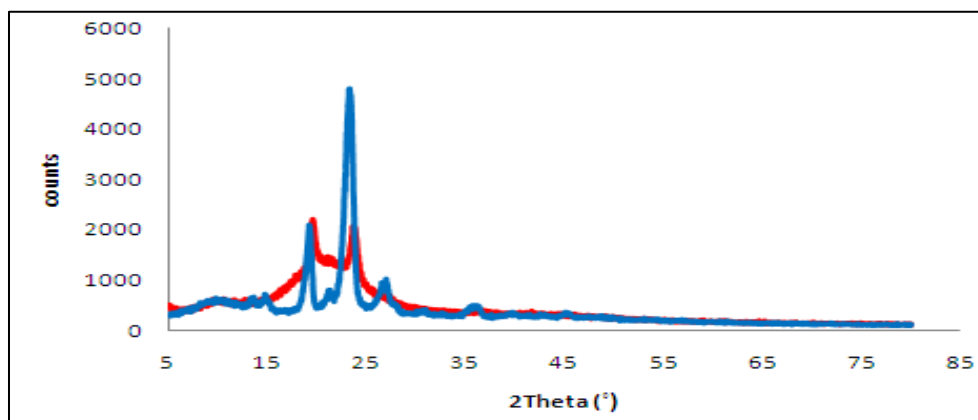


Figure 3.28. XRD patterns of PEO-2K (blue) and PEO2-UU30 (red).

PEO2-UU30 nanocomposites, where a fairly broad peak at $2\theta = 22^\circ$ instead of two very sharp peaks at $2\theta = 20^\circ$ and $2\theta = 25^\circ$ clearly indicates that the fumed silica addition disrupts the crystalline of the poly(ethylene oxide) matrix. As the amount of silica filler is increased the peak becomes weaker and broader.

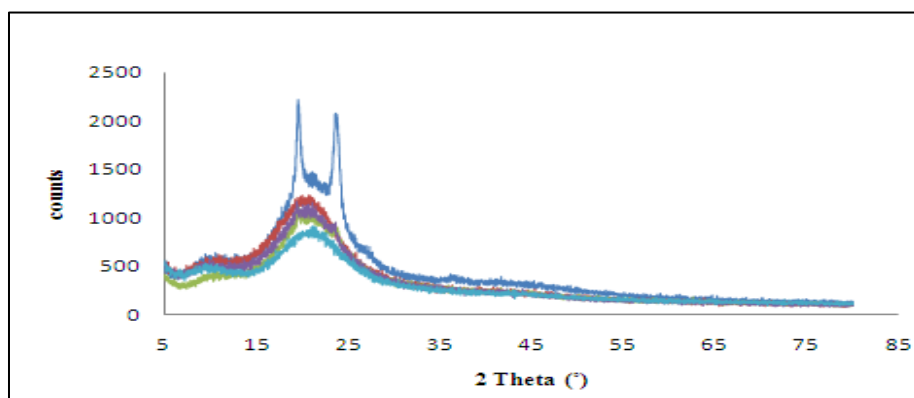


Figure 3.29. XRD Patterns of PEO2-UU30 (blue), and nanocomposites with HDK H2K 5% (red), 10% (green), 20% (purple) and 40% (light blue)

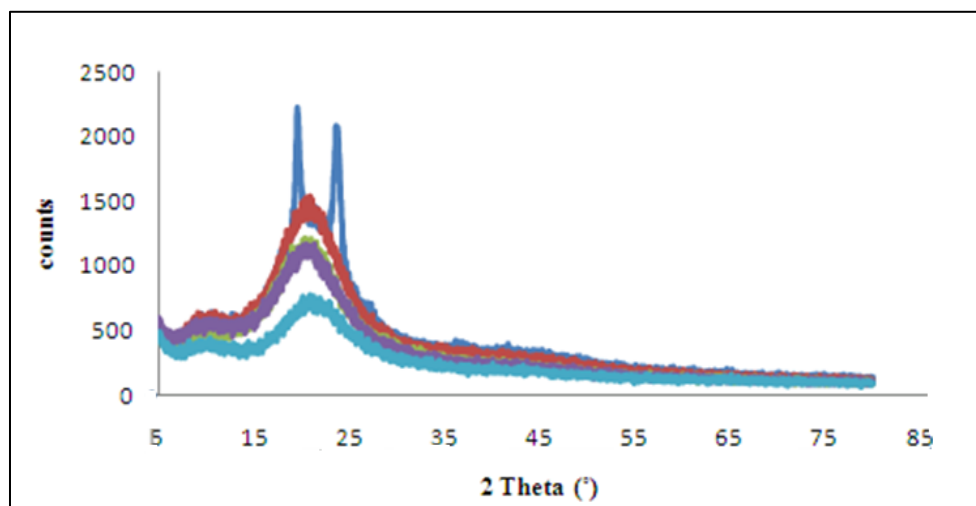


Figure 3.30. XRD Patterns of PEO2-UU30 (blue) and nanocomposites with HDK N20. 5% (red), 10% (green), 20% (purple) and 40% (light blue).

As shown in Figures 3.31. and 3.32. poly(tetramethylene oxide) based polyurethaneurea PTMO2-UU20 had a broad peak at $2\theta = 20^\circ$ with a shoulder at $2\theta = 10^\circ$. These peaks corresponded to the partially crystalline nature of the polymer matrix. Upon fumed silica addition (HDK H2K or HDK N20), the intensity of the two peaks decreased irrespective of whether fumed silica is hydrophilic or hydrophobic, which can be seen on Figures 3.31. and 3.32. respectively for H2K and N20. The decrease was more pronounced in higher fumed silica loadings. These results indicate that fumed silica incorporation affects the crystallinity of the polymer matrix.

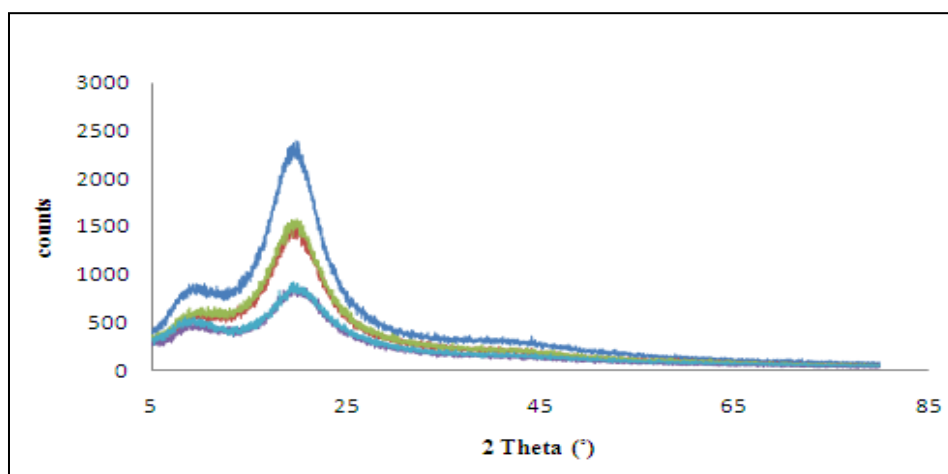


Figure 3.31. XRD patterns of PTMO2-UU20 (blue), and nanocomposites with HDK H2K. 5% (red), 10% (green), 20% (purple) and 40 % (light blue).

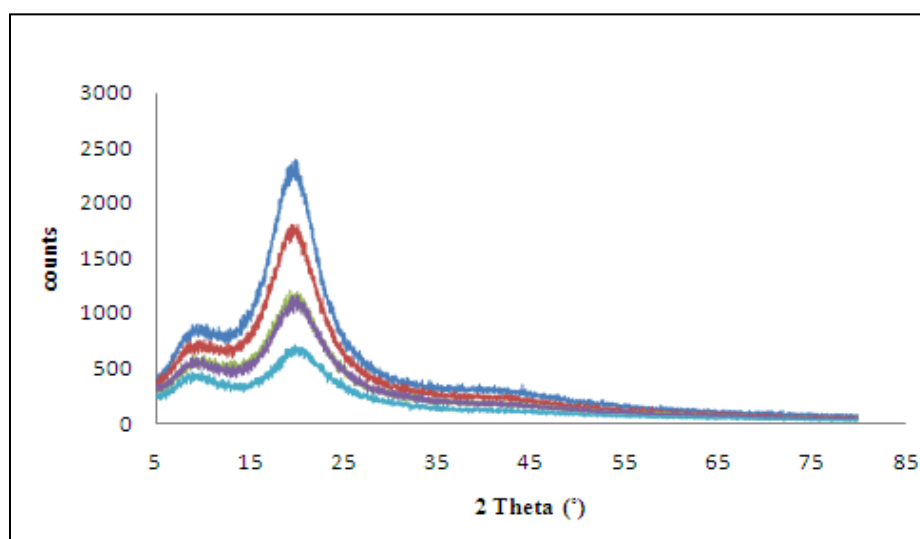
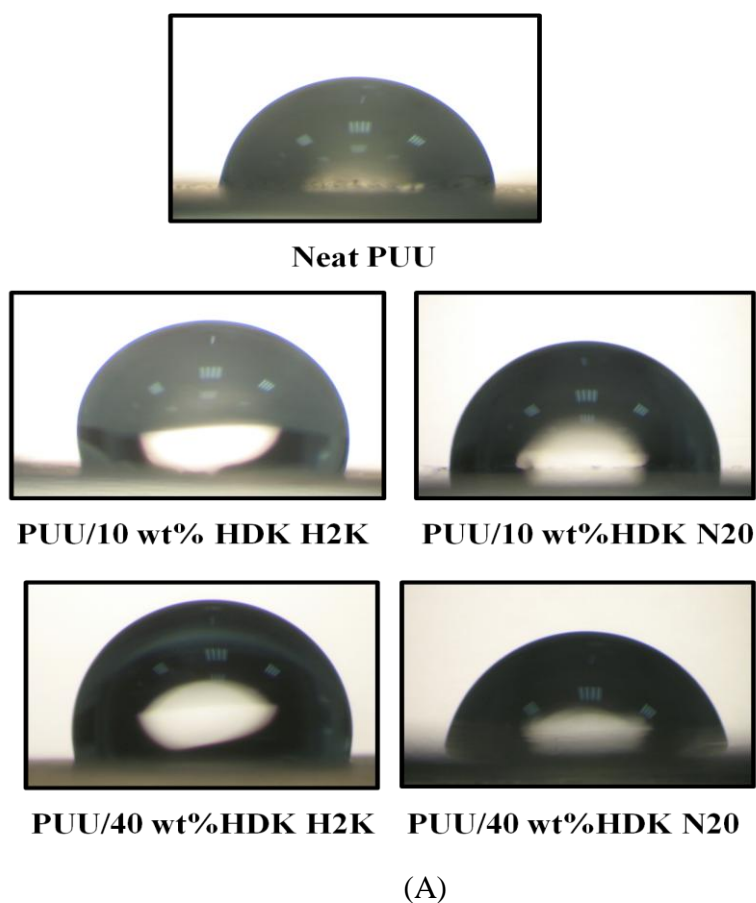


Figure 3.32. XRD patterns of PTMO2-UU20 (blue), and nanocomposites with HDK N20. 5% (red), 10% (green), 20% (purple) and 40 % (light blue).

3.6. Contact Angle Studies of Neat Polymers and Fumed Silica-Polymer

Nanocomposites

In order to understand the effect of silica addition on the surface properties of the polymeric composites, static water contact angles on the air side of the host polymers and nanocomposite films were measured. During the measurements of 20 μL of deionized, triple distilled water was used. Pictures of the water droplets on the air surface of PTMO2-UU20 copolymer and various nanocomposites are reproduced in Figure 3.33. Average results of 10 measurements on the static water contact angles of PTMO and PDMS based copolymers and their nanocomposites are reproduced on Table 3.7.



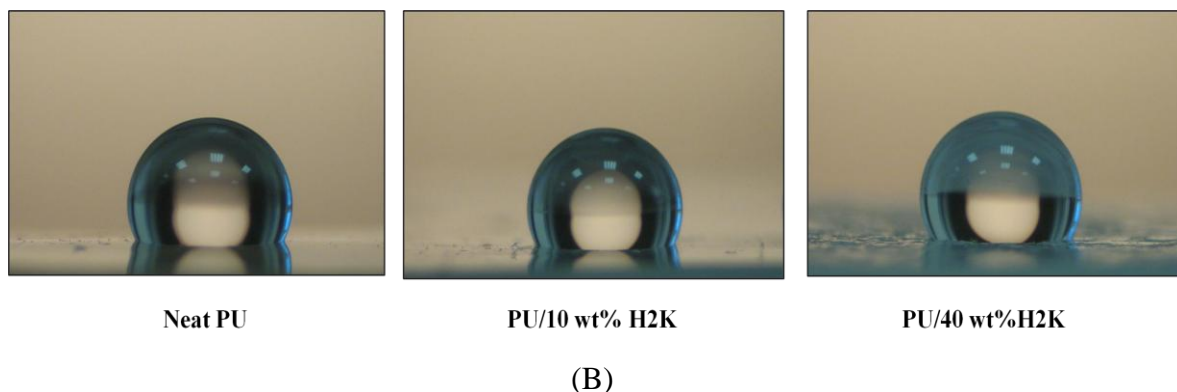


Figure 3.33. Static water contact angles on air surfaces of (A) PTMO2-UU20 and its nanocomposites and (B) PDMS32-U5 and its nanocomposites

Increase in contact angle of PTMO2-UU20 nanocomposites with respect to the neat copolymer may indicate that surface roughness of the PTMO based nanocomposites seem to increase by the incorporation of both hydrophobic and hydrophilic fumed silica. However, as the fumed silica content was increased from 10 to 40 weight % contact angle decreased slightly, which may be due to the homogenous distribution of the fumed silica clusters throughout the matrix.

Table 3.7. Static water contact angles on PTMO2-UU20 and PDMS32-U5 copolymers and their nanocomposites containing 10 and 40 weight % of fumed silica

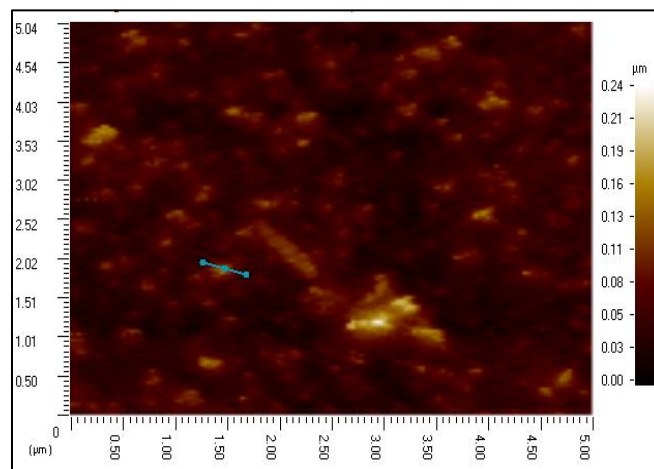
	Polymer	HDK H2K		HDK N20	
		10 wt%	40 wt%	10 wt%	40 wt%
PTMO2-UU20	77.1 ± 2.1	98.7 ± 1.4	89.4 ± 1.7	93.1 ± 2.3	80.5 ± 1.1
PDMS32-U5	110.6 ± 2.3	115.3 ± 1.6	112.4 ± 1.6	--	--

In case of PEO2-UU30 copolymer and its nanocomposites, it was difficult to measure the static water contact angles since the polymer was extremely hydrophilic and deformation of the contact area occurred due to immediate swelling of the polymer making the measurements irreproducible. After 5 minutes the water drop was absorbed causing a temporary deformation on the polymer surface. Unlike the nanocomposites prepared with poly(tetramethylene oxide) based polyurethaneureas, no trend in contact angle was achieved due to the swelling of the surface.

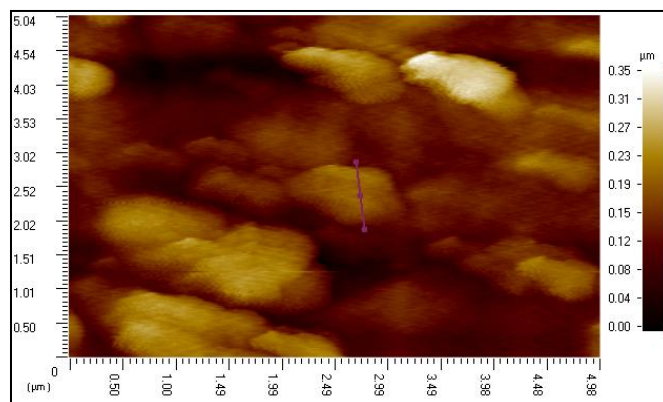
As well known from the literature [48, 49] silicone-urea copolymers display very hydrophobic surfaces with contact angles above 100°. As provided on Table 3.7., PDMS32-U5 displayed a contact angle of 110°, which slightly increased to 115° in its nanocomposite containing 10 weight percent of hydrophobic silics H2K, which may be due to the increased surface roughness. In case of the nanocomposite containing 40 weight percent of H2K, the contact angle did not show much of a change.

3.7. Atomic Force Microscopy Studies

Tapping mode AFM measurements were performed to investigate the topographic features and the spatial variation on the surface by height and phase imaging. The scales of the AFM phase images were set so that the harder phase appeared darker in the phase images, whereas the higher parts appeared lighter in the height images. Height images reflected surface morphology, whereas phase images provided a sharp contrast of structural features and emphasized differences in mechanical properties of different sample components. Therefore, the roughness analysis was performed on the height images with dimensions of 5 X 5µm. Figures 3.34. and 3.35. provide the AFM phase and height images for, PEO2-UU30 and PTMO2-UU20 copolymers and their silica nanocomposites.

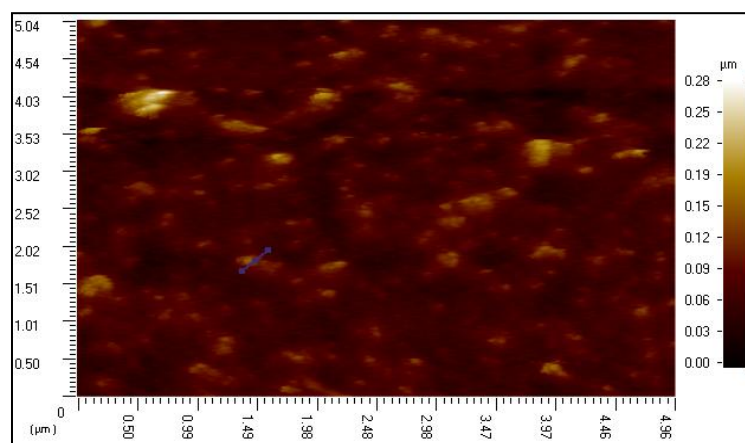


(A)

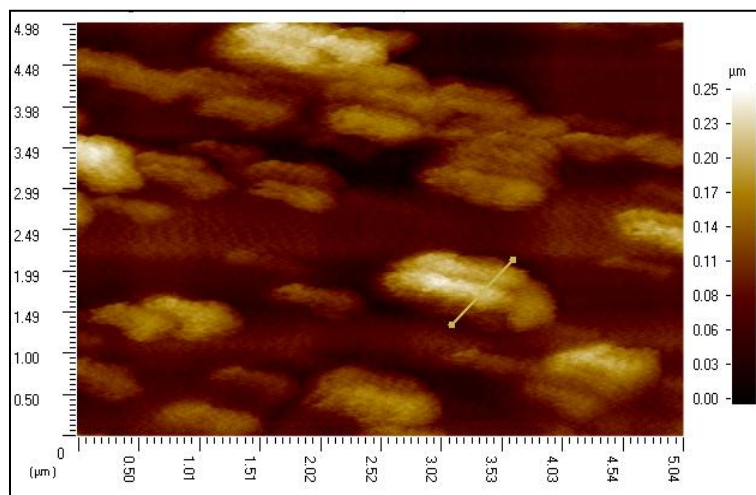


(B)

Figure 3.34. AFM Height Images of (A) PEO2-UU30/10wt% HDK H2K and (B) PEO2-UU30/ 10 wt% HDK N20



(A)



(B)

Figure 3.35. AFM Height Images of (A) PTMO2-UU20/10wt% HDK H2K and (B) PTMO2-UU30/10 wt% HDK N20

The height image of both pure PEO2-UU30 and PTMO2-UU20 have root-mean-square roughness below 1 nm, indicating that the film surfaces were smooth. However, in case of nanocomposites prepared by 10 weight % of hydrophobic or hydrophilic fumed silica, root-mean-square roughness values increased significantly due to the bulges on the surfaces

representing clusters of fumed silica. The findings of the AFM study correlated with those of the contact angle measurements performed on the same polymer and nanocomposites. We were also able to measure the cross-section and height of the fumed silica clusters. The height and the cross-section values of the fumed silica agglomerates under the crosssection lines are shown in Table 3.8.

Table 3.8. Height and crosssection values of selected fumed silica agglomerates in the nanocomposites

	PEO2-UU30		PTMO2-UU20	
	10wt%HDK H2K	10wt%HDK N20	10wt%HDK H2K	10wt%HDK N20
height (nm)	100	100	100	150
Cross-section (nm)	300	1000	300	900

As can be seen from the table, silica agglomerates rather than aggregates were found in the matrix. Moreover, hydrophilic fumed silica tend to agglomerate more than hydrophobic fumed silica. This finding coincided with the results of our DLS studies.

3.8. Influence of Fumed Silica Filler on the Tensile Properties of the Nanocomposites

One of the main aims of preparing silica filled polymeric composites or nanocomposites is to improve their mechanical properties, such as the modulus and the ultimate tensile strength. As a result we performed detailed investigation of the tensile properties of nanocomposites produced. A summary of the tensile properties of PEO2-UU30 and its

nanocomposites with hydrophilic and hydrophobic silica are summarized on Table 3.9., where, (M) (TS) and (E) denote Young's modulus, ultimate tensile strength and elongation at break values. As can be seen from Table 3.9., PEO2-UU30 displays fairly nice elastomeric properties with a modulus of about 7 MPa, ultimate tensile strength of about 28 MPa and elongation at break slightly over 1000%. Interestingly, incorporation of up to 20% by weight of hydrophobic silica (HDK H2000) does not seem to influence the properties, especially the modulus and the tensile strength of the materials. There seems to be a slight reduction in elongation at break. At 40% loading of HDK H2000, the modulus seems to go up, which is expected, but there is a significant reduction in the ultimate tensile strength, which is somewhat unexpected. This may be due to the interaction of the silica with urea groups which disrupts the strong hydrogen bonding, as observed from FTIR spectra and discussed previously.

Table 3.9. Tensile properties of PEO2-UU30 and its nanocomposites

Sample description	M (MPa)	TS (MPa)	E (%)
PEO2-UU30	5.6 ± 0.9	27.2± 4.5	1150 ± 7
PEO2-UU30/5wt%HDK H2K	4.0 ± 2.1	28.1 ± 1.4	965 ± 16
PEO2-UU30/10%HDK H2K	4.34 ± 3.2	27.7 ± 2.1	911 ± 13
PEO2-UU30/20%HDK H2K	7.1 ± 1.2	27.1 ± 4.7	861 ± 106
PEO2-UU30/40wt%HDK H2K	16.2 ± 3.0	21.6 ± 0.5	1143 ± 2
PEO2-UU30	5.6 ± 0.9	27.2± 4.5	1150 ± 7
PEO2-UU30/5wt%HDK N20	5.1 ± 0.5	23.2 ± 0.7	987 ± 8
PEO2-UU30/10wt%HDK N20	9.6 ± 2.2	29.3 ± 1.3	1050 ± 7
PEO2-UU30/20wt%HDK N20	20.1 ± 4.8	22.3 ± 7.9	1153 ± 150
PEO2-UU30/40wt%HDK N20	21.7 ± 3.6	20.8 ± 1.7	1063 ± 80

As can be seen from Table 3.9, a very similar trend in tensile properties were observed in nanocomposites containing hydrophilic silica HDK N20. Fumed silica in the range of a few tens of nanometers was expected to act like hard segments in the polymer matrix and reinforce the material. But, in our case, as shown by AFM studies, fairly large silica agglomerates were present in the matrix rather than single silica particles. From the tensile tests results we believe such agglomerates in micrometer size were too large in size in comparison to the hard segment domains. Additionally, they may not have enough surface area to interact with the matrix. We believe the decrease in tensile strength at high silica loadings can be explained by: (i) the interaction of some of the hydrophilic silica particles with the urea hard segments, disrupting the hydrogen bonding in the system, and (ii) the presence of large agglomerates which does not act as reinforcing agent.

In contrast to our findings, it was seen in literature that introduction of filler into an elastomeric network increases strength but decreases extensibility. As mentioned above, the reinforcement effect depends strongly on the size of filler particles, with maximum reinforcement being obtained for filler particles with small sizes since they cause more extended configurations for the chains in the network. Moreover, random, regular, and aggregated particle dispersions are needed for improving the mechanical properties

By the size of the filler particles we mean relative size of the particle to the chain length of the polymers. Besides acting as hard segments and reinforcing the matrix, filler particles with sizes in nanometer range also increase the dimensions of the chains when the filler particles are small relative to the dimensions of the network chains. Moreover, chains are more stretched with an increase in the amount of smaller filler particles. In contrast, particles that are relatively large tend to decrease the chain dimensions. In our case,

agglomerated structures with micron sizes, may have also decreased the chain dimensions leading to worsened mechanical properties. [50, 51, 52, 53]

In PTMO2-UU20 based nanocomposites both hydrophilic and hydrophobic fumed silica additions raised the initial modulus slightly with respect to the neat polymer, whereas no effect on the tensile strength was observed (Table 3.10.). However, 40 weight % loading again decreases tensile strength significantly. Again in this case agglomerates rather than fumed silica particles may be the reason of the trend in tensile properties. These clusters disrupted the crystallinity of the polymer matrix as shown in the previous studies.

In case of silicone-urea copolymers, however, fumed silica addition improved mechanical properties of the nanocomposites with respect to the neat polymer. As can be seen in Table 3.10., nanocomposites exhibited gradual increase in Young's modulus, tensile strength and percent elongation with increasing hydrophobic fumed silica addition. Unlike in case of polyether-based polyurethaneureas, fumed silica addition enhanced the tensile properties of silicone-urea based nanocomposites indicating a synergistic interaction between filler and the matrix.

Table 3.10. Tensile properties of PTMO2-UU20 copolymer and its nanocomposites

Component	M (MPa)	TS (Mpa)	E (%)
PTMO2-UU20	3.6 ± 0.1	28.6 ± 2.2	900 ± 5
PTMO2-UU20/5wt%HDK H2K	4.5 ± 0.4	26.9 ± 1.9	815 ± 20
PTMO2-UU20/10wt%HDK H2K	4.7 ± 0.3	25.7 ± 4.6	820 ± 45
PTMO2-UU20/20wt%HDK H2K	7.6 ± 0.2	26.6 ± 3.9	735 ± 10
PTMO2-UU20/40wt%HDK H2K	5.8 ± 0.9	19.3 ± 2.3	945 ± 95
PTMO2-UU20	3.6 ± 0.1	28.6 ± 2.2	900 ± 5
PTMO2-UU20/10wt%HDK N20	3.8 ± 0.2	14.4 ± 1.3	1440 ± 32
PTMO2-UU20/40wt%HDK N20	21.3 ± 3.1	17.7 ± 0.6	993 ± 30

Table 3.11. Tensile properties of PDMS32-U5 copolymer and its nanocomposites

component	M (MPa)	TS (MPa)	E (%)
PDMS32-U5	1.1	0.85 ± 0.03	650 ± 2
PDMS32-U5/10wt%HDK H2K	2.25 ± 0.10	0.95 ± 0.06	200 ± 11
PDMS32-U5/20wt%HDK H2K	6.10 ± 0.10	1.40 ± 0.02	110 ± 2

Chapter 4

Conclusions

Commercially available hydrophobic (HDK H2000) and hydrophilic (HDK N20) fumed silica from Wacker Chemie were used for the preparation of polyurethaneurea based nanocomposites. Three different polyurethaneurea copolymers based on PTMO-2000, PEO-2000 and PDMS-32000 were synthesized in our laboratories. Nanocomposites containing up to 40% by weight of fumed silica were prepared by solution blending. Neat polymers and the nanocomposites were characterized by a large number of techniques in order to understand the influence of the silica type and amount on the morphology and tensile properties of segmented polyurethaneureas.

Extensive spectroscopic studies by FTIR and ATR-IR on model compounds and nanocomposites revealed that incorporation of fumed silica somewhat hindered the strongly hydrogen bonded urea and urethane networks in polyether (PEO and PTMO) based segmented copolymers. There was no difference in the H-bonding characteristics of the urea groups in segmented silicone-urea copolymers upon silica incorporation. Addition of fumed silica also affected the packing characteristics of the polyether soft segment chains. Poly(ethylene oxide) and poly(tetramethylene oxide) oligomers had partial crystallinity, which was disrupted by the addition of silica. These results made us to conclude that fumed silica addition changed the morphology of the whole matrix in case of polyether based systems whereas the morphology of silicone-urea copolymer nanocomposites were less affected.

Tensile properties of silicone-urea based nanocomposites were enhanced upon fumed silica addition, whereas there was almost no difference in the tensile properties of polyether based nanocomposites with respect to the neat polymer, regardless of the amount or type of silica incorporation.

BIBLIOGRAPHY

- [1] Fukushima Y, Inagaki S. J. Inclusion Phenomena 1987; 5: 473–482.
- [2] Fukushima Y, Okada A, Kawasumi M, Kurauchi T, Kamigaito O. Clay Minerals 1988; 23: 27–34
- [3] Usuki A, Kojima Y, Kawasumi M, Okada A, Fukushima Y, Kurauchi T, Kamigaito O. J. Materials Research 1993; 8: 1179–1184.
- [4] Yılgör E, Burgaz E, Yılgör I. Polymer 2000; 41: 849-857
- [5] Das S, Cox DF, Wilkes GL, Klinedinst DB, Yılgör I, Yılgör E, Beyer FL. J. Macromolecular Sci. Part B: Physics 2007; 46: 853-875
- [6] Yılgör E, Yılgör I. Polymer 2001; 42: 7953-7959
- [7] Otterstedt OE, Ekdahl J, Backman J. J. Polymer Sci. 1987; 34: 2575-2582
- [8] Tien YU, Wei KH. J. Polymer Sci. 2002; 86: 1741-1748
- [9] Lee HS, Wang YK, Hsu SL. Macromolecules 1987; 20(9): 2089-2095
- [10] Synder, MD, US Pat., 2,623,031 (1952)
- [11] Schollenberger CS, US Pat., 2,871,218 (1959)
- [12] Yılgör E, Tulpar E, Kara Ş, Yılgör I. ACS Symposium Series, 729, Chapter 26, 395-407
- [13] Paquien JN, Galy J, Gerard JF, Pouchelon A. Colloids and Surfaces 2005; 260: 165-172
- [14] Yılgör I, Eynur T, Yılgör E, Wilkes GL. Polymer 2009; 50: 4432-4437
- [15] Vansant EF. “*Characterization and Chemical Modification of the Silica Surface*”, Vol. 93, Elsevier, New York, 1995
- [16] Aranguren MI, Mora E, Macosko CW. J. Colloids and Interfaces Sci. 1997; 195: 329-337
- [17] http://www.wacker.com/cms/media/publications/downloads/6178_EN.pdf

- [18] Boonstra BB, Cochrane H, Dannenberg EM. “*Reinforcement of Silicone Rubber by Particulate Silica*”, International Rubber Conference, Munich Germany 1974.
- [19] http://www.wacker.com/cms/media/publications/downloads/6176_EN.pdf
- [20] Barus S, Zanetti M, Lazzari M, Costa L. *Polymer* 2009; 50: 2595-2600
- [21] DeGroot JV, Macosko CW, J. *Colloids and Interfaces Sci.* 1999; 217: 86-93
- [22] Koo JH. “*Polymer Nanocomposites: Processing, characterization and applications*”, McGraw-Hill, New York, 2006
- [23] Beloqui BJ, Garcia JCF. *J. Adhesion Sci. Technol.* 1999; 13(6): 695-711
- [24] Petrovic ZS, Javni I, Waddon A, Banhegyi G. *J. App. Pol. Sci.* 1999; 76: 133-151
- [25] Nunes RCR, Fonseca JLC, Pereira MR: *Polymer Testing* 2000; 19: 93-103
- [26] Filippone G, Romeo G, Acierno D. *Langmuir* 2010; 26(4): 2714-2720
- [27] Arrighi V, Higgins JS, Burgess AN, Floudas G. *Polymer* 2001; 39(25): 6369-6376
- [28] Bokobza L. *Macromol Symp* 2001; 169: 243-260
- [29] Sharaf MA, Mark JE. *Polymer* 2004; 45: 3943-3852
- [30] Kim GM, Michler GH. *Polymer* 1998; 39(23): 5689-5697
- [31] Mele P, Marceau S, Brown D, Puydt Y, Alberola ND. *Polymer* 2002; 43: 5577-5586
- [32] Cosgrove T, Turner MJ, Thomas DR. *Polymer* 1997; 38(15): 3885- 3892
- [33] Tsagaropoulos G, Eisenberg A. *Macromolecules* 1995; 28: 396-398
- [34] Tsagaropoulos G, Eisenberg A. *Macromolecules* 1995; 28: 6067-6077
- [35] Gagliardi S, Arrighi V, Ferguson R, telling MTF. *Physica B* 2001; 301: 110-114
- [36] Gee RH, Maxwell RS, Balazs B. *Polymer* 2004; 45: 3885-3891
- [37] Serbescu A, Saalwachter K. *Polymer* 2009;50(23):5434-5442
- [38] Mackay ME, Tuteja A, Duxbury PM, Hawker CJ, Van Horn B, Guan ZB, Chen GH, Krishnan RS. *Science* 2006; 311(5768):1740-1743
- [39] Matsuura H, Tatsuo M. *Polymer* 1969; 7: 1735-1744
- [40] Kuroda Y, Kubo K. *Polymer* 1957; 16: 323-328

-
- [41] Kuroda Y, Kubo K. *Polymer* 1959; 36: 435-439
- [42] Shen Z, Simon GR, Chen Y. *Polymer* 2002; 43: 4251-4260
- [43] Yilgor E, Yilgor I, Das S, Wilkes G. J. *Polymer Sci. Part B* 2009; 47: 471-483
- [44] Pizzatto L, Lizot A, Fiorio R. *Materials Sci. Eng.* 2009; 29: 474-478
- [45] Gun'ko VM, Yurchenko GR, Turov VV. *J. Colloid Interface Sci.* 2010; 348: 546-558
- [46] Anastasescu C, Anastasescu M, Teodorescu VS. *J. Non-crystalline Solids* 2010; 356: 2634-2640
- [47] Chen Y, Shuxue Z, Yang H. *J. Colloid Interface Sci.* 2004; 279: 370-378
- [48] Yilgor E, Yilgor I, Suzer S. *J. App. Polymer Sci.* 2002; 83: 1625-1634
- [49] Yilgor E, Yilgor I, Suzer S. *Polymer* 2003; 44: 7271-7279
- [50] Yuan QW, Kloczowski A, Mark JE. *Polymer* 1996; 34: 1647-1657
- [51] Pu Z, Mark JE. *Chem. Matter* 1997; 9: 2442-2447
- [52] Paul DR, Mark JE. *Progress Polymer Sci.* 2010; 35: 893-901
- [53] Mark JE. *Mol. Cryst. Liq. Cryst.* 2002; 374: 29-38

VITA

Çağla Koşak was born in Izmir, Turkey on March 4, 1985. She received her B. Sc. degree in Chemistry from Bogazici University, Turkey in 2009. From September 2009 to August 2011 she worked as a teaching and research assistant with full scholarship in Koc University, Turkey. She is working in Tübitak Research Project about “Investigation of Interactions between Polymer and Nanoparticle in Silica- filled, Polyether- based Nanocomposites.